Pairing mean-field theory for the dynamics of dissociation of molecular Bose-Einstein condensates

M. J. Davis,[1] S. J. Thwaite,[1,2] M. K. Olsen,[1] and K. V. Kheruntsyan[1]
[1]*ARC Centre of Excellence for Quantum-Atom Optics, School of Physical Sciences, University of Queensland, Brisbane, Queensland 4072, Australia*
[2]*Department of Physics, University of Auckland, Auckland, New Zealand*
(Received 23 October 2007; published 15 February 2008)

We develop a pairing mean-field theory to describe the quantum dynamics of the dissociation of molecular Bose-Einstein condensates into their constituent bosonic or fermionic atoms. We apply the theory to one-, two-, and three-dimensional geometries and analyze the role of dimensionality on the atom production rate as a function of the dissociation energy. As well as determining the populations and coherences of the atoms, we calculate the correlations that exist between atoms of opposite momenta, including the column density correlations in three-dimensional systems. We compare the results with those of the undepleted molecular field approximation and argue that the latter is most reliable in fermionic systems and in lower dimensions. In the bosonic case we compare the pairing mean-field results with exact calculations using the positive-*P* stochastic method and estimate the range of validity of the pairing mean-field theory. Comparisons with similar first-principle simulations in the fermionic case are currently not available, however, we argue that the range of validity of the present approach should be broader for fermions than for bosons in the regime where Pauli blocking prevents complete depletion of the molecular condensate.

DOI: 10.1103/PhysRevA.77.023617 PACS number(s): 03.75.Mn, 03.75.Kk, 03.65.−w, 05.30.−d

I. INTRODUCTION

The generation and detection of strongly correlated atomic ensembles is becoming one of the central themes in the study of ultracold quantum gases, leading to the birth of the subfield of quantum-atom optics. Recently there have been an increasing number of experiments probing the higher-order coherences and correlation functions that are fundamental to this field and are analogous to similar developments in the early days of quantum optics with photons.

One of the first experiments in this area was the measurement of a two-time second-order correlation function in a thermal gas of metastable neon atoms falling on four microchannel plate (MCP) detectors [1]. Another early experiment was the measurement of the rate of three-body losses from a Bose-Einstein condensate (BEC), from which the local third-order correlation function could be inferred [2] (see also [3]). More recently, the arsenal of experimental techniques to study higher-order correlations has been expanded to include the measurement of photoassociation rates [4], shot-noise spectroscopy of absorption images [5–8], atom counting using fluorescence imaging, and high-finesse optical cavities [9,10], and position-resolved counting of metastable helium atoms using arrays of MCP detectors [11–13]. Proposals for additional techniques include atom counting using photoionization [14], and freeze-in techniques with optical lattices for *in-situ* measurements of nonlocal spatial correlations [15].

The experimental systems that are being studied with these new techniques for correlation measurements include Bose-Einstein condensates and degenerate Fermi gases [2,11,12], atom lasers [10], one-dimensional (1D) and quasi-1D Bose gases [3,4,8,9], Bose and Fermi gases in optical lattices [6,7], four-wave mixing via BEC collisions [13], and molecular dissociation of BECs [5]. The last two systems are relevant to the present work and have similar atom-atom correlations on the dissociation sphere and on the *s*-wave scattering halo, respectively [16,17]. All the experiments described above generate quantum correlations that cannot be described by Gross-Pitaevskii mean-field theory. They provide a challenge for theorists to develop and apply more advanced techniques in order to quantitatively model experimental systems, such as used in Refs. [16,18–26].

Particular interest in molecular dissociation experiments stems from the prospect of generating and detecting squeezed states of matter waves [18,19,27–31], with potential applications in precision measurements. There also exists the possibility of producing Einstein-Podolsky-Rosen correlations and other entangled states of massive particles [32–39] for fundamental tests of quantum theory in mesoscopic regimes and for quantum information science applications. Additionally, molecular dissociation can serve as a probe of two-body interactions, collisional resonances, and spectroscopic properties of Feshbach resonance molecules [40–43]. Other recent studies of dissociation are concerned with the role of confinement on the stability of a molecular BEC against dissociation [44], the effect of magnetic field fluctuations on dissociation [45], and the dynamics of molecule-atom conversion in optical lattices [46].

The purpose of this paper is to develop and apply a pairing mean-field theory (PMFT) to the dynamics of dissociation of a BEC of molecular dimers consisting of pairs of either bosonic or fermionic atoms. The mean fields for the molecules are introduced in the standard way at the level of amplitudes, whereas for the atoms they are introduced at the level of pairing fields [47] that describe normal and anomalous moments of the atomic creation and annihilation operators. This approach takes into account the molecular depletion and can facilitate the calculation of atom-atom pair correlation functions beyond the coherent level of the simple mean-field theory. The present PMFT is similar to that of Jack and Pu [23], except that (i) we extend the analysis to one-dimensional and two-dimensional (2D) systems; (ii) we relax the approximation of the constant density of atomic

 ©2008 The American Physical Society

states around the peak dissociation energy; and (iii) we calculate the pair correlation functions for dissociated atoms.

First-principle quantum simulations of the dissociation of molecular BECs into bosonic atoms have been performed using the stochastic positive-P representation method [18,19,24], however, this technique has some limitations. Most significant is the short time scale over which the positive-P method remains valid and produces results free of large sampling errors or the boundary term problem [48]. For pure dissociation, without s-wave scattering interactions, the typical time scale for the positive-P simulations is limited to about 50% conversion [24]. The addition of s-wave scattering interactions further limits this to even shorter durations and only 5%–10% conversion for typical experimental parameters [24]. The situation is less clear in the fermionic case; even though similar first-principle techniques for simulating multimode fermion dynamics have recently been developed [49], these techniques have not been applied yet to the problem of multimode dissociation for quantitative comparison.

Given the limitations of exact techniques, it is useful to develop alternative, approximate theoretical techniques that can deal with longer durations of dissociation and larger conversion percentage. The PMFT developed here and in Ref. [23] falls into this category and goes beyond previous approximate theories that ignore molecular depletion altogether [24,50]. As such, the range of its validity with respect to molecular depletion covers dissociation durations corresponding to near complete conversion. In addition, the PMFT is able to treat the dissociation into bosonic and fermionic atoms on equal footing and therefore is closer to being able to quantitatively describe the experiments on dissociation of $^{40}K_2$ dimers into fermionic atoms [5], in addition to the earlier experiments on dissociation of $^{23}Na_2$ [51] and $^{87}Rb_2$ [52] dimers into bosonic atoms.

This paper is organized as follows. In Sec. II we introduce the model Hamiltonians describing the dissociation into distinguishable and indistinguishable atoms and discuss the validity of approximations involved in our model. In Sec. III we give the simplest possible description of dissociation based on a Fermi's golden rule calculation of the molecular decay rate and discuss the implications for dissociation in 1D, 2D, and three-dimensional (3D) geometries. In Sec. IV we develop the PMFT and discuss our main results for dissociation dynamics, atomic momentum distribution, and atom-atom correlations. Our conclusions are summarized in Sec. VI.

II. MODEL

In our treatment of dissociation we assume an initial condition of a stationary BEC of diatomic molecules consisting of either (i) two distinguishable fermionic or bosonic atoms (e.g., in two different spin states) or (ii) two indistinguishable bosonic atoms. In the case (i), we further assume that both constituents are of the same species and have the same mass; we do not consider heteronuclear molecules. The model Hamiltonians for each of these situations are described below, and we discuss the initial conditions and the validity of our approximations in Sec. II C.

A. Dissociation into distinguishable atoms

The quantum field theoretic effective Hamiltonian describing the system in one, two, or three ($D=1,2,3$) spatial dimensions is given, in a rotating frame, by [53]

$$\hat{H}=\int d^D\mathbf{x}\left(\sum_{i=0,1,2}\frac{\hbar^2}{2m_i}|\nabla\hat{\Psi}_i|^2+\hbar\Delta(\hat{\Psi}_1^\dagger\hat{\Psi}_1+\hat{\Psi}_2^\dagger\hat{\Psi}_2)-i\hbar\chi_D(\hat{\Psi}_0^\dagger\hat{\Psi}_1\hat{\Psi}_2-\hat{\Psi}_2^\dagger\hat{\Psi}_1^\dagger\hat{\Psi}_0)\right). \quad (1)$$

The molecular field is described by a bosonic operator $\hat{\Psi}_0(\mathbf{x},t)$ while the two atomic fields are described by either bosonic or fermionic operators $\hat{\Psi}_1(\mathbf{x},t)$ and $\hat{\Psi}_2^\dagger(\mathbf{x},t)$. The field operators satisfy the respective commutation or anticommutation relations, i.e., $[\hat{\Psi}_i(\mathbf{x},t),\hat{\Psi}_j^\dagger(\mathbf{x}',t)]=\delta_{ij}\delta^{(D)}(\mathbf{x}-\mathbf{x}')$ in the case of bosonic atoms or $\{\hat{\Psi}_i(\mathbf{x},t),\hat{\Psi}_j^\dagger(\mathbf{x}',t)\}=\delta_{ij}\delta^{(D)}(\mathbf{x}-\mathbf{x}')$ $(i=1,2)$ in the fermionic case. For notational simplicity, we use $\mathbf{x}$ for the position in 1D, 2D, and 3D cases, with the understanding that in the 1D case it is a scalar.

The first term in the Hamiltonian (1) describes the kinetic energy where the atomic masses are $m_1=m_2$, whereas the molecular mass is $m_0=m_1+m_2=2m_1$. The coupling term χ_D is responsible for coherent conversion of molecules into atom pairs, e.g., via optical Raman transitions or a Feshbach resonance sweep (see, for example, Refs. [47,53–58] and [59,60] for recent reviews). For the Raman case, the coupling χ_{3D} is expressed in terms of the Rabi frequencies for free-bound and bound-bound transitions as in Ref. [55].

In the case of a Feshbach resonance, the coupling χ_{3D} is given by (see [47,56,57] for notational consistency)

$$\chi_{3D}=\sqrt{4\pi a_{bg}\Delta\mu\Delta B/m_1}. \quad (2)$$

Here $\Delta\mu=\mu_1+\mu_2-\mu_0$ is the difference in the magnetic moments of the atomic and the bound molecular states, ΔB is the magnetic width of the resonance, and a_{bg} is the background scattering length for s-wave collisions of the atoms in the two spin states. In systems of reduced dimensionality (1D or 2D) and away from confinement-induced resonances, the couplings χ_{1D} and χ_{2D}, are obtained by integrating over the ground-state wave function in the tightly confined dimensions. Assuming harmonic trapping potentials in the eliminated dimensions, with oscillation frequencies $\omega_\perp\equiv\omega_y=\omega_z$ in the 1D case and ω_z in the 2D case, the respective atom-molecule couplings are

$$\chi_{1D}=\chi_{3D}/(2\pi l_\perp^2)^{1/2}, \quad (3)$$

$$\chi_{2D}=\chi_{3D}/(2\pi l_z^2)^{1/4}. \quad (4)$$

Here $l_\perp=\sqrt{\hbar/m_1\omega_\perp}$ and $l_z=\sqrt{\hbar/m_1\omega_z}$ are the harmonic oscillator lengths for the atoms. For a given transverse trap frequency $\omega_\perp$ in the 1D geometry, the dissociation detuning must satisfy $|\Delta|<\omega_\perp$ to avoid transverse excitations and maintain the validity of the 1D treatment. Similarly, in the 2D case one must satisfy $|\Delta|<\omega_z$ in order that the system remains in the 2D regime in the xy plane.

The quantity Δ in the Hamiltonian (1) is the effective detuning between the molecular state with energy E_0 and the

atomic states with energies E_1 and E_2. It is defined differently depending on whether the coupling is due to a sweep through a Feshbach resonance, or due to Raman photoassociation lasers.

(i) In the Feshbach resonance case, dissociation of an initially stable ($E_0 < E_1+E_2$) molecular BEC into the constituent atoms may be achieved by a rapid magnetic field sweep onto the atomic side of the resonance ($E_0 > E_1+E_2$) [52]. The detuning is defined as the overall energy mismatch $2\hbar\Delta = E_1+E_2-E_0$ between the free two-atom state in the dissociation threshold with energy E_1+E_2 and the bound molecular state of energy E_0. The sweep is implemented to result in a finite and negative detuning $2\hbar\Delta<0$ after the sweep ($E_0 > E_1+E_2$), in which case the molecules become unstable against spontaneous dissociation into free atom pairs.

(ii) In the case of two-photon Raman photoassociation [19,55], the overall energy mismatch is given by $2\hbar\Delta = E_1 + E_2 - E_0 - \hbar\omega$, where ω is the frequency difference between the two Raman lasers. Similarly, for an rf transition [5] ω is the rf frequency.

In all our numerical examples, we assume that the dissociation energy $2\hbar|\Delta|$ is much larger than the energy shift due to the renormalization [47,57], which allows us to equate the parameters in the equations of motion with their observed values.

The Hamiltonian (1) conserves the total number of atomic particles

$$\hat{N} = 2\hat{N}_0(t) + \hat{N}_1(t) + \hat{N}_2(t) = \text{const}, \tag{5}$$

where the constant is given by $2\hat{N}_0(0)$ for the vacuum initial condition for the atoms.

B. Dissociation into indistinguishable atoms

Molecular dissociation into pairs of indistinguishable bosonic atoms in the same internal state is described by the following Hamiltonian [54], in a rotating frame:

$$\hat{H} = \int d^D\mathbf{x}\left(\sum_{i=0,1} \frac{\hbar^2}{2m_i}|\nabla\hat{\Psi}_i|^2 + \hbar\Delta\hat{\Psi}_1^\dagger\hat{\Psi}_1 - i\frac{\hbar\chi_D}{2}(\hat{\Psi}_0^\dagger\hat{\Psi}_1^2 - \hat{\Psi}_1^{\dagger 2}\hat{\Psi}_0)\right), \tag{6}$$

where $\hat{\Psi}_1(\mathbf{x})$ is the atomic field operator, and χ_D is the atom-molecule coupling. The microscopic expression for the 3D coupling χ_{3D} in the case of a Feshbach resonance is given by [47,56,57]

$$\chi_{3D} = \sqrt{8\pi a_{bg}\Delta\mu\Delta B/m_1}, \tag{7}$$

where a_{bg} is the atom-atom background scattering length, $\Delta\mu = 2\mu_1 - \mu_0$ is the magnetic moment difference between the atomic and the bound molecular states, and ΔB is the magnetic width of the resonance. For systems of reduced dimensionality, Eqs. (3) and (4) for χ_{1D} and χ_{2D} are unchanged.

The Hamiltonian (6) conserves the total number of atomic particles

$$\hat{N} = 2\hat{N}_0(t) + \hat{N}_1(t) = \text{const}, \tag{8}$$

where the constant is given by $2\hat{N}_0(0)$ for the vacuum initial condition for the atoms.

C. Initial conditions and approximations

Starting with a stable molecular condensate, we assume that the coupling χ_D is switched on in the regime of a sudden jump [43]; initially the molecules are assumed to be in a coherent state, whereas the atomic fields are in the vacuum state. The energy level configuration after the Feshbach sweep or the Raman transitions (corresponding to $\Delta<0$) is the actual initial condition for our simulations.

For a molecule at rest, the excess of potential energy $2\hbar|\Delta|$ (which we also refer to as the dissociation energy) is converted into kinetic energy $2\hbar^2k^2/(2m_1)$ of atom pairs with equal but opposite momenta $\pm\mathbf{k}_0$, where $k_0 = |\mathbf{k}_0| = \sqrt{2m_1|\Delta|}/\hbar$. This is the physical origin of the expected correlations between the atoms, which we will study below in the context of many-body field theory.

The main limitation of our treatment is that we consider a spatially uniform system in a cubic box with periodic boundary conditions. The question that one must address then is how well the results of a uniform model can describe realistic nonuniform systems. It has previously been shown [24] that while the uniform treatment can give quantitatively reasonable results for the total number of atoms and the atomic density distribution (provided the uniform system is appropriately size matched to a nonuniform system, as in Sec. IV A 1), such a treatment is not adequate for giving correct quantitative results for density-density correlation functions. The reason is the mode mixing due to inhomogeneity of trapped condensates, which can strongly degrade the correlations compared to the predictions of the uniform model [24]. Nevertheless, the merit of calculating the correlation functions here is that the results provide upper bounds for the correlations [24,50] and hence aid qualitative understanding.

Another obvious consideration when applying the uniform results to size-matched nonuniform systems is that the duration of dissociation should not exceed the time required for the atoms to propagate distances larger than the size of the uniform box L. Thus the results are valid for times

$$t \lesssim t_{\max} = \frac{L}{v_0} = L\sqrt{m_1/(2\hbar|\Delta|)}, \tag{9}$$

where $v_0 = \hbar k_0/m_1$ is the mean velocity of the dissociated atoms. In other words, while our numerical results can be formally obtained for arbitrarily long times, the above equation should be used to cutoff these results at $t_{\max}$ when they are applied to a specific nonuniform system of size L.

The next major assumption in our treatment is the mean-field coherent state for molecules at all times [23]. This approximation breaks down once the dissociation approaches the regime of complete depletion of the molecular condensate ($\sim$100% conversion) when quantum fluctuations become increasingly important. Accordingly, the results of the mean-field theory cannot be trusted past that point in time; we present these results only for academic purposes. We note

that nearly complete conversion in the mean-field theory would always take place in the case of bosonic atoms, but not necessarily in the fermionic case where the Pauli exclusion principle for the atoms can dominate the molecular depletion. In this situation the fermionic results can prove to be reliable for longer durations than in the bosonic case.

Finally, we do not include any *s*-wave scattering interaction terms. Potentially these interactions can affect the atom-atom correlations in realistic nonuniform systems, especially in the long time limit. However, their effect is negligible at low particle densities and short dissociation times [24]. At the level of mean fields, the *s*-wave scattering terms can be neglected if the dissociation energy is much larger than the mean-field interaction energy. More importantly, it has been shown in Ref. [24] that the strongest degradation of atom-atom correlations in realistic systems (compared to the predictions of uniform models) comes not from the *s*-wave scattering interactions, but from the mode mixing due to inhomogeneity. Accordingly, any theory that attempts to give quantitatively correct results for atom-atom correlations must first address the question of inhomogeneity before including *s*-wave interactions. The pairing mean-field theory developed here does not have this goal, but represents an intermediate step between the simple analytic theory of undepleted molecules [24,50] and a more complete theory that can reliably treat mode mixing due to inhomogeneity and *s*-wave scattering interactions for both bosonic and fermionic atoms.

III. DECAY RATE AND DISSOCIATION DYNAMICS FROM FERMI'S GOLDEN RULE

A. Distinguishable atoms

Before presenting our numerical results within the framework of the PMFT, we discuss the simpler results that follow from a Fermi's golden rule calculation of the molecular decay rate. Due to the conservation of the total number of atomic particles, the molecular decay rate can be converted into the rate of atom production and serve as the simplest description of the dynamics of dissociation in the initial spontaneous regime. In particular, Fermi's golden rule gives the correct initial behavior of the total atom number as a function of time since at this stage neither bosonic stimulation nor Pauli blocking affects the dynamics of individual modes. It also provides simple and useful insights into the differences associated with the dimensionality of the system, which are not explicit in the numerical results. The derivation presented here is a direct calculation based on the actual many-body Hamiltonian rather than an estimate based on the comparison of the mean-field energy shift and the energy shift of a Feshbach resonance state as in Ref. [51].

According to Fermi's golden rule, the molecular decay rate Γ is given by [51,61]

$$\Gamma = \frac{2\pi}{\hbar}|V_{ma}|^2 D^{(2)}(\epsilon), \tag{10}$$

where $D^{(2)}(\epsilon)$ is the density of two-atom states, ϵ is the total kinetic energy of two atoms corresponding to the total dissociation energy $\epsilon = 2\hbar|\Delta|$, and V_{ma} is the transition matrix element for the atom-molecule coupling channel. Calculating V_{ma} explicitly from the interaction Hamiltonian in Eq. (1) (see Appendix A for details), we obtain the following results in one, two, and three dimensions:

$$\Gamma = \begin{cases} \lambda\chi_{1D}^2/|\Delta|^{1/2} & (1D), \\ \lambda^2\chi_{2D}^2 & (2D), \\ 2\lambda^3\chi_{3D}^2|\Delta|^{1/2}/\pi & (3D), \end{cases} \tag{11}$$

where $\lambda = (m_1/2\hbar)^{1/2}$ is a constant. Since each molecule produces two atoms (one per spin state) we can treat the decay rate Γ as the atom production rate using the conserved total particle number $2N_0(t)+N_1(t)+N_2(t)=2N_0(0)=\text{const}$. Here, $N_i=\langle\hat{N}_i\rangle$ with $N_0(0)$ being the total initial number of molecules with no atoms present. Thus, the solution $N_0(t)=N_0(0)\exp(-\Gamma t)$ to the rate equation for the molecular decay, can be rewritten as $N_1(t)+N_2(t)=2N_0(0)[1-\exp(-\Gamma t)]$. Noting also that $N_1(t)=N_2(t)$ since $\hat{N}_1-\hat{N}_2$ is conserved, the final result for the total number of atoms in each spin state takes the following simple form:

$$N_{1(2)}(t) = N_0(0)(1-e^{-\Gamma t}) \simeq N_0(0)\Gamma t \quad (\Gamma t \ll 1). \tag{12}$$

We see immediately that the atom production rate in 1D, 2D, and 3D increases, remains unchanged, and decreases, respectively, with the dissociation energy $2\hbar|\Delta|$, following the respective dependence of the decay rate Γ on the detuning $|\Delta|$. This is a direct consequence of the different dependence of the density of atomic states $D(E)$ on energy E in 1D, 2D, and 3D.

B. Indistinguishable atoms

The decay rate Γ derived above is for dissociation into distinguishable atoms. For completeness, we now present the derivation in the case of indistinguishable (bosonic) atoms and show that the resulting expression in 3D coincides with the expression given in Ref. [51]. The reasons for presenting these details are twofold. First, we would like to point out that even though the present paper is primarily concerned with dissociation into distinguishable atom pairs (either fermions or bosons in different spin states), the results in the bosonic case can be easily modified to describe the case of indistinguishable atoms in the same spin state. Second, we would like to spell out the connection of the microscopic Feshbach parameters with the coupling constant χ_{3D} in the respective field-theory Hamiltonians without leaving room for confusion about "factors of 2." The details of derivation of the decay rate Γ' in the present case are given in Appendix B; the final result is

$$\Gamma' = \begin{cases} \lambda\chi_{1D}^2/2|\Delta|^{1/2} & (1D), \\ \lambda^2\chi_{2D}^2/2 & (2D), \\ \lambda^3\chi_{3D}^2|\Delta|^{1/2}/\pi & (3D). \end{cases} \tag{13}$$

For the same coupling strength χ_D these rates appear to be simply one-half the corresponding result for the distinguishable case, Eq. (11). However, one must take into account that the interaction Hamiltonian for the present indistinguishable

case has an extra factor of 1/2 in front of χ_D and that the definition of χ_D in the two cases are different.

The total number of atoms produced during the initial stage of dissociation ($\Gamma' t \ll 1$) is

$$N_1(t) = 2N_0(0)(1 - e^{-\Gamma' t}) \simeq 2N_0(0)\Gamma' t \quad (\Gamma' t \ll 1). \tag{14}$$

Comparing this with the result of Eq. (12) we see that for the same coupling constant χ_D in the Hamiltonians (6) and (1), the total number of atoms produced in the indistinguishable case corresponds to the number of atoms in each spin state produced in the distinguishable case.

IV. PAIRING MEAN-FIELD THEORY

A. Distinguishable atoms

Considering a uniform system in a cubic box of volume $V=L^3$ (or a square of area $A=L^2$ in 2D, or a line of length L in 1D), we expand the molecular and atomic field operators in terms of plane-wave modes,

$$\hat{\Psi}_0(\mathbf{x},t) = \frac{1}{L^{D/2}} \sum_{\mathbf{k}} \hat{b}_{\mathbf{k}}(t) e^{i\mathbf{k}\cdot\mathbf{x}}, \tag{15}$$

$$\hat{\Psi}_j(\mathbf{x},t) = \frac{1}{L^{D/2}} \sum_{\mathbf{k}} \hat{a}_{j,\mathbf{k}}(t) e^{i\mathbf{k}\cdot\mathbf{x}}, \tag{16}$$

where $\hat{b}_{\mathbf{k}}(t)$ and $\hat{a}_{j,\mathbf{k}}(t)$ $(j=1,2)$ are the corresponding creation operators satisfying the usual bosonic commutation relation for molecules $[\hat{b}_{\mathbf{k}}, \hat{b}^{\dagger}_{\mathbf{k}'}] = \delta_{\mathbf{k},\mathbf{k}'}$ and fermionic anticommutation or bosonic commutation relations for the atoms, $\{\hat{a}_{i,\mathbf{k}}, \hat{a}^{\dagger}_{j,\mathbf{k}'}\} = \delta_{\mathbf{k},\mathbf{k}'}\delta_{i,j}$ or $[\hat{a}_{i,\mathbf{k}}, \hat{a}^{\dagger}_{j,\mathbf{k}'}] = \delta_{\mathbf{k},\mathbf{k}'}\delta_{i,j}$. Here $\mathbf{k} = (2\pi/L)\mathbf{n}$ is the momentum in wave-number units, with $\mathbf{n} = (n_x, n_y, n_z)$ and $n_i = 0, \pm 1, \pm 2, \ldots$ $(i=x,y,z)$ in the 3D case, with similar relations in the 1D and 2D cases.

The Hamiltonian of the system, Eq. (1), can now be written as

$$\hat{H} = \sum_{\mathbf{k}} \frac{\hbar^2 \mathbf{k}^2}{2m_0} \hat{b}^{\dagger}_{\mathbf{k}} \hat{b}_{\mathbf{k}} + \sum_{\mathbf{k},j=1,2} \left(\frac{\hbar^2 \mathbf{k}^2}{2m_j} + \hbar\Delta \right) \hat{a}^{\dagger}_{j,\mathbf{k}} \hat{a}_{j,\mathbf{k}}$$
$$- i\frac{\hbar\chi_D}{L^{D/2}} \sum_{\mathbf{q},\mathbf{k}} (\hat{b}^{\dagger}_{\mathbf{q}} \hat{a}_{1,\mathbf{k}} \hat{a}_{2,\mathbf{q}-\mathbf{k}} - \hat{a}^{\dagger}_{2,\mathbf{q}-\mathbf{k}} \hat{a}^{\dagger}_{1,\mathbf{k}} \hat{b}_{\mathbf{q}}). \tag{17}$$

To proceed, we next assume that the initial condition is a large molecular condensate in the mode $\hat{b}_0$ $[\langle \hat{b}^{\dagger}_0(0)\hat{b}_0(0)\rangle \gg 1]$ and that the dynamics of dissociation retains the molecular population in the same condensate mode $\hat{b}_0(t)$. This implies that we ignore any atom-atom recombination process in which two atoms with nonopposite momenta $\hat{a}_{1,\mathbf{k}}$ and $\hat{a}_{2,\mathbf{q}-\mathbf{k}}$ combine to populate a noncondensate molecular mode $\hat{b}_{\mathbf{q}}$ with $\mathbf{q} \neq 0$. This is a reasonable approximation at least during the initial stages of dissociation when recombination is negligible. Thus, the Hamiltonian (17) now reduces to

$$\hat{H} = \sum_{\mathbf{k}} \hbar\Delta_{\mathbf{k}} (\hat{a}^{\dagger}_{1,\mathbf{k}} \hat{a}_{1,\mathbf{k}} + \hat{a}^{\dagger}_{2,\mathbf{k}} \hat{a}_{2,\mathbf{k}})$$
$$- i\hbar\kappa \sum_{\mathbf{k}} (\hat{b}^{\dagger}_0 \hat{a}_{1,\mathbf{k}} \hat{a}_{2,-\mathbf{k}} - \hat{a}^{\dagger}_{2,-\mathbf{k}} \hat{a}^{\dagger}_{1,\mathbf{k}} \hat{b}_0), \tag{18}$$

where we have introduced $\Delta_{\mathbf{k}} \equiv \Delta + \hbar\mathbf{k}^2/(2m_1)$ and a new coupling constant

$$\kappa \equiv \chi_D / L^{D/2}. \tag{19}$$

We note that the Hamiltonian (18) conserves the total number of atomic particles, $\hat{N} = 2\hat{b}^{\dagger}_0\hat{b}_0 + \Sigma_{\mathbf{k}}(\hat{n}_{1,\mathbf{k}} + \hat{n}_{2,\mathbf{k}})$, and the number difference, $\hat{n}_{1,\mathbf{k}} - \hat{n}_{2,\mathbf{k}}$, where $\hat{n}_{j,\mathbf{k}} = \hat{a}^{\dagger}_{j,\mathbf{k}}\hat{a}_{j,\mathbf{k}}$ $(j=1,2)$ are the particle number operators for the atoms.

The next step in the mean-field approach is to assume that the molecular condensate is initially in a coherent state with an amplitude β_0 $[\langle \hat{b}^{\dagger}_0(0)\hat{b}_0(0)\rangle = |\beta_0|^2 \gg 1]$, and that it remains in a coherent state during the dynamical evolution. The condensate dynamics are then treated at the level of the mean-field amplitude, $\beta(t) = \langle \hat{b}_0(t)\rangle$, which implies that we can approximate the higher-order correlation function $\langle \hat{b}^{\dagger}_0 \hat{a}_{1,\mathbf{k}} \hat{a}_{2,-\mathbf{k}}\rangle \approx \beta^*_0 \langle \hat{a}_{1,\mathbf{k}} \hat{a}_{2,-\mathbf{k}}\rangle$. Thus, the decorrelation assumption is imposed at all times, which is the main limitation of the method. This treatment will become increasingly inadequate as the molecular population depletes and approaches zero.

Once we impose the decorrelation assumption, the dynamics of the atomic fields can be described in terms of the normal and anomalous populations

$$n_{\mathbf{k}}(t) \equiv \langle \hat{n}_{1,\mathbf{k}}(t)\rangle = \langle \hat{n}_{2,\mathbf{k}}(t)\rangle, \tag{20}$$

$$m_{\mathbf{k}}(t) \equiv \langle \hat{m}_{\mathbf{k}}(t)\rangle = \langle \hat{a}_{1,\mathbf{k}}(t) \hat{a}_{2,-\mathbf{k}}(t)\rangle, \tag{21}$$

which describe the occupation numbers of the atomic modes with momenta $\mathbf{k}$, Eq. (20), and the correlation between the modes with equal but opposite momenta, $\mathbf{k}$ and $-\mathbf{k}$, in the two spin states, Eq. (21). In this description, higher-order correlation functions factorize according to Wick's theorem, i.e., they can be expressed in terms of the second-order moments $n_{\mathbf{k}}(t)$ and $m_{\mathbf{k}}(t)$.

Writing the Heisenberg operator equations of motion following from the Hamiltonian (18) and imposing the pairing mean-field decorrelation approximation, one can show that the equations of motion for the scaled mean-field amplitude,

$$f(\tau) \equiv \beta(t)/\beta_0, \tag{22}$$

and the normal and anomalous populations $n_{\mathbf{k}}(t)$ and $m_{\mathbf{k}}(t)$ form a closed set and can be written as

$$\frac{dn_{\mathbf{k}}(\tau)}{d\tau} = m^*_{\mathbf{k}}(\tau) f(\tau) + m_{\mathbf{k}}(\tau) f^*(\tau),$$

$$\frac{dm_{\mathbf{k}}(\tau)}{d\tau} = -2i\delta_{\mathbf{k}} m_{\mathbf{k}}(\tau) + f(\tau)[1 \pm 2n_{\mathbf{k}}(\tau)],$$

$$\frac{df(\tau)}{d\tau} = -\frac{1}{\beta_0^2}\sum_{\mathbf{k}} m_{\mathbf{k}}(\tau). \tag{23}$$

In these equations and throughout the rest of this paper, the upper (lower) sign refers to bosonic (fermionic) atom statistics, and we have introduced dimensionless time $\tau = t/t_0$ and dimensionless effective detuning

$$\delta_{\mathbf{k}} = \Delta_{\mathbf{k}} t_0 = [\hbar \mathbf{k}^2/(2m_1) + \Delta]t_0 = q^2 + \delta, \tag{24}$$

where $t_0 = 1/(\kappa\beta_0)$ is the time scale (where we have assumed that β_0 is real without loss of generality), $q = |\mathbf{q}|$ is the absolute value of the dimensionless momentum $\mathbf{q} = \mathbf{k}d_0$, $d_0 = \sqrt{\hbar t_0/(2m_1)}$ is the length scale, and $\delta = \Delta t_0$ is the dimensionless bare detuning. The quantity $f(\tau)$ is the fractional molecular amplitude so that $|f(\tau)|^2 = N_0(\tau)/N_0(0)$ corresponds to the fraction of molecules relative to their initial total number. Equations (23) conserve the quantity $|m_{\mathbf{k}}(t)|^2 - n_{\mathbf{k}}(t)[1 \pm n_{\mathbf{k}}(t)]$ as its time derivative is zero, and so the normal and anomalous densities are directly related according to

$$|m_{\mathbf{k}}(t)|^2 = n_{\mathbf{k}}(t)[1 \pm n_{\mathbf{k}}(t)]. \tag{25}$$

This will be useful in the calculation of correlation functions in Sec. V B.

Equations (23) are equivalent to those solved in Ref. [23] for describing dissociation dynamics in 3D using spin-1/2 Pauli matrices [62]. Here, we extend this treatment to 1D and 2D systems. In addition, we analyze the second-order correlation functions for the atoms and give detailed quantitative assessment of the approximations involved in the pairing mean-field method compared to the exact first-principles treatment using the positive-P representation for bosons [24].

1. Results for total atom numbers

In Figs. 1 and 2 we show typical results from solving Eqs. (23) for fermionic and bosonic atom statistics, respectively. We plot the fraction of the total number of atoms in each spin component relative to the total initial number of molecules, $N_{1,2}(\tau)/N_0(0)$, as a function of time. The two graphs, (a) and (b), are for two different values of the dimensionless detuning $\delta = \Delta t_0$ ($\delta < 0$) and the same initial dimensionless molecular density $N_0(0)/l^D = 3.1$ ($D = 1,2,3$), where $l = L/d_0$ is the dimensionless length corresponding to the quantization length L.

These parameters can be size matched with a realistic nonuniform system corresponding, for example, to a BEC of molecular dimers made of fermionic ^{40}K atoms as in Ref. [5]. Our empirically derived prescription for the size matching [24] is as follows. Assuming for simplicity an isotropic harmonically trapped molecular condensate with a Thomas-Fermi parabolic density profile, we match the parameters of the present uniform treatment to have the same peak density ρ_0 as the trapped condensate and choose the length L of the uniform box to result in the same initial total number of molecules as in the trapped condensate $N_0(0) = (8\pi/15)R_{\mathrm{TF}}^3\rho_0 = L^3\rho_0$, where R_{TF} is the Thomas-Fermi radius. Thus, the length L is size matched to $L^3 = (8\pi/15)R_{\mathrm{TF}}^3$ [24,50]. Taking the peak density $\rho_0 = 7.6 \times 10^{18}$ m^{-3}, the trap frequency $\omega/2\pi = 52$ Hz, and molecule-molecule scattering length $a_{mm} \simeq 1.47$ μm in the strongly interacting regime near a magnetic Feshbach resonance, we obtain $R_{\mathrm{TF}} = \sqrt{8\pi\hbar^2 a_{mm}\rho_0/m_0^2\omega^2} \simeq 33.1$ μm, $L \simeq 39.3$ μm, and a total number of molecules $N_0(0) \simeq 3 \times 10^5$. Assuming a 3D atom-molecule coupling $\chi_{3\mathrm{D}} = 4.87 \times 10^{-7}$ m$^{3/2}$ s^{-1}, we obtain a time scale of $t_0 = 1/[\kappa\sqrt{N_0(0)}] \simeq 0.918$ ms, where $\kappa = \chi_{3\mathrm{D}}/L^{3/2} \simeq 1.98$ s^{-1} and giving a length scale of $d_0 \simeq 0.854$ μm, $l = L/d_0 \simeq 46$, and hence $N_0(0)/l^3 \simeq 3.1$.

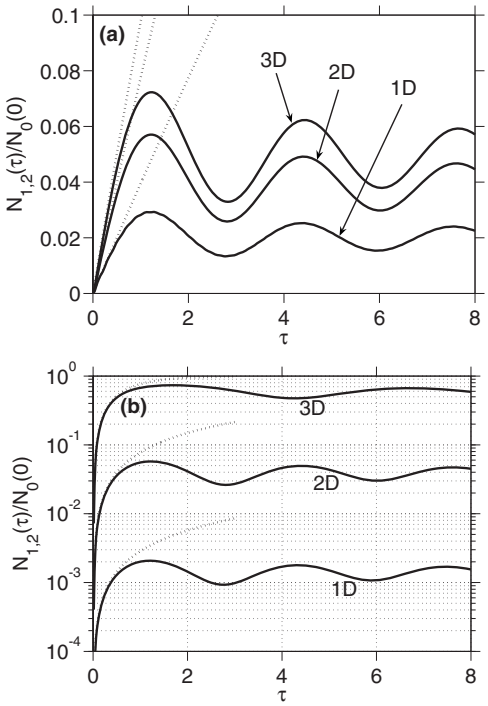

FIG. 1. Dissociation of a molecular condensate into fermionic atoms. We plot the total number of atoms in each spin component $N_{1,2}(\tau)$ [$N_1(\tau) = N_2(\tau)$] relative to the total initial number of molecules $N_0(0)$ as a function of the dimensionless time $\tau = t/t_0$, where $t_0 = 1/\kappa\sqrt{N_0(0)}$ is the time scale. The graphs (a) and (b) are for $|\delta| = 16$ and $|\delta| = 3174$, respectively. The different curves are for 1D, 2D, and 3D cases as shown. In all cases, the initial dimensionless molecular density is $N_0(0)/l^D = 3.1$ ($D = 1,2,3$), where $l = L/d_0$ is the dimensionless length. The dotted lines next to each solid line are the results from Fermi's golden rule, Eqs. (11) and (12). See text for further details.

Most of the numerical examples given here are for two values of the dimensionless detuning, $|\delta| = 16$ and $|\delta| = 3174$, where $\delta = \Delta t_0$. Using the above time scale of $t_0 \simeq 0.918$ ms, these detunings correspond to $|\Delta|/2\pi \simeq 3.67$ kHz and $|\Delta|/2\pi \simeq 0.55$ MHz. The second case is chosen to coincide with the average rf detuning of $\nu_{\mathrm{rf}} = 1.1$ MHz used in the experiment of Ref. [5], where we note that ν_{rf} corresponds to the absolute detuning of $|\Delta|/\pi$ in our notation. The duration of dissociation of 0.33 ms used in Ref. [5] corresponds to dimensionless time of $\tau \simeq 0.36$ at which our 3D results give $N_1(t)/N_0(0) \simeq 0.39$ (39% conversion), in good agreement with ~43% conversion obtained in Ref. [5]. We also note that the dimensionless time $\tau_{\max} = l/(2\sqrt{|\delta|})$ corresponding to Eq. (9) is equal to $\tau_{\max} \simeq 0.41$ in this example, which is larger than the dissociation duration of $\tau \simeq 0.36$ as required

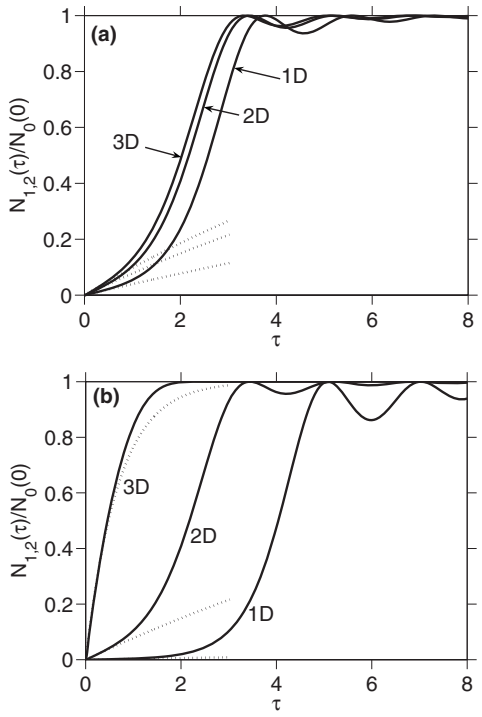

FIG. 2. Dissociation of a molecular condensate into distinguishable bosons. Apart from bosonic statistics, all parameters are the same as for Fig. 1.

for the applicability of the uniform treatment.

More detailed quantitative comparison with the results of Ref. [5], especially those for the momentum distribution and atom-atom correlations, is complicated by the fact that the detuning $\nu_{\rm rf}$ was swept over 600 kHz during the experiment in order to spread the detected signal over many camera pixels. We do not model the rf sweep in the present work. Additional discrepancies are expected to arise due to the fact that the trap geometry in the experiment was not spherically symmetric as assumed here.

The results of Figs. 1 and 2 are easily understood using the dependence of the density of atomic states on energy, Eq. (A5). By energy and momentum conservation, the total dissociation energy $2\hbar|\Delta|$ is converted into the kinetic energy, $2\hbar|\Delta| \to \hbar^2 k_\uparrow^2/(2m_1) + \hbar^2 k_\downarrow^2/(2m_1)$, of atom pairs with opposite spins and momenta. The atomic momenta are distributed in a narrow interval around $k_0 = |\mathbf{k}_{\uparrow(\downarrow)}| = \sqrt{2m_1|\Delta|/\hbar}$. In 3D, the resonant momenta form a spherical shell with a radius k_0; in 2D they are distributed within a circular shell at the same radius, while in 1D the resonant momenta are around $\pm k_0$. Since the density of atomic states at the dissociation energy is the largest in 3D, the number of dissociated atoms is larger in 3D than in 2D and 1D.

Next, we address the question of how the number of dissociated atoms changes with the dissociation energy $2\hbar|\Delta|$. Since the density of states increases with energy in 3D, a larger absolute detuning results in a larger number of atoms produced [compare the 3D curves in Figs. 1(a) and 1(b); also in Figs. 2(a) and 2(b)]. In 1D the situation is reversed; the density of states decreases with energy and hence the number of atoms at a given time is smaller at larger absolute detuning $|\Delta|$. In 2D, the density of states is independent of the energy and we see no variation of the total atom number with the detuning. Indeed, the 2D curves in Figs. 1 and 2 are indistinguishable within numerical accuracy, even though the equations were solved with different detunings.

As expected, the dependencies on the absolute detuning in 1D, 2D, and 3D found numerically are in agreement with the explicit analytic results for the atom production rate found from Fermi's golden rule, Eq. (12). The atom numbers from the simple rate equation (12) are shown by dotted lines in Figs. 1 and 2, where they appear as the tangents to the respective numerical results at $\tau \to 0$.

Comparing the results of the pairing mean-field theory with those based on Fermi's golden rule calculations of the molecular decay rate, we see that in the initial spontaneous stage of dissociation the bosonic and fermionic results are very similar. Past the spontaneous regime, the dynamics of dissociation becomes affected by either Pauli blocking or bosonic stimulation, depending on the statistics of the dissociated atoms. Accordingly, the fermionic results for the total atom number saturate faster and lie below the curve corresponding to the simple rate equation, while the bosonic results exhibit exponential growth due to Bose enhancement and remain above the rate equation curve.

In the bosonic case, the ultimate limit to the growth in atom number is set by the total (finite) initial number of molecules as the condensate can be entirely depleted. For fermions, however, the Pauli exclusion principle—depending on dimensionality of space and absolute detuning—can take effect before there is any significant depletion of the molecular condensate. In this sense the molecular depletion is a more important factor in the bosonic case than in the fermionic case. This situation applies to all curves in Fig. 1(a) and to 1D and 2D results in Fig. 1(b). In all these fermionic cases the conversion efficiency is less than 8% during the entire simulation time and the molecular depletion is negligible. Accordingly, the dynamics of dissociation follows closely the predictions obtained within the undepleted molecular field approximation of Ref. [50]. This is shown in Fig. 3(a), where we present the comparison in the 3D case, where the discrepancy is the largest. Owing to the different dependencies of the density of states on the absolute detuning in different dimensions, the undepleted molecular field approximation works better at small absolute detunings in 3D and at large detunings in 1D. For the same reason, the molecular depletion generally is less important in 1D than in 3D.

If, on the other hand, the number of available atomic states in the spherical shell around k_0 [see Eq. (35) for the width of the shell] is comparable to or larger than the total initial number of molecules, then the dynamics of dissociation is dominated by the molecular field depletion. In this case, the number of molecules can decrease substantially before the population of individual atomic modes experiences any Pauli blocking. This is a typical situation in 3D at very large absolute detunings $|\delta|$ when there is a large number of states available for occupancy. Even if the average occupation of each of these states is smaller than one, the total average number of atoms can be quite large and constitute a large fraction of the initial number of molecules. Accordingly, the predictions of the undepleted molecular field ap-

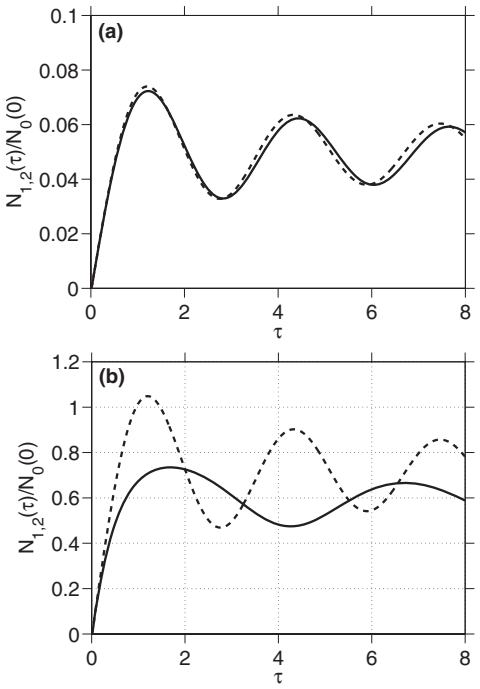

FIG. 3. Same as in Figs. 1(a) and 1(b) in the 3D case, except that the results of the pairing mean-field theory (solid lines) are compared with those obtained within the undepleted molecular field approximation (dashed line).

proximation remain valid only for a very short time as seen in Fig. 3(b). In the longer time limit, the undepleted molecular field approximation leads to an unphysical result that the fractional atomic population becomes larger than one, as seen in Fig. 3(b). This situation is similar to the well-known behavior in the bosonic case (see Fig. 5 below).

2. Parametrization at large dissociation energy

Once the equations of motion are written in dimensionless form it is clear that the system can be described via just two parameters—the dimensionless detuning δ and the initial number of molecules $N_0=\beta_0^2$. The quantization volume drops out of the final results if we are interested in fractional populations or normalized densities rather than their absolute values.

For large dissociation energy (large absolute detuning, $|\delta|\gg 1$), the parametrization of the system can be further simplified and reduced to just one parameter which is a function of N_0 and $|\delta|$ [23]. Here, we show this for the case of distinguishable atoms and note that the same arguments apply to the indistinguishable case. As shown in Appendix C, the parameter in question originates from the approximate form of Eqs. (23) in the continuous limit, which gives the following equation for the fractional amplitude:

$$\frac{df(\tau)}{d\tau} \simeq -\sqrt{\frac{2}{\Upsilon}}\int_{-\infty}^{\infty} d\delta_k m(\delta_k,\tau). \tag{26}$$

Here, the dimensionless parameter Υ is defined via

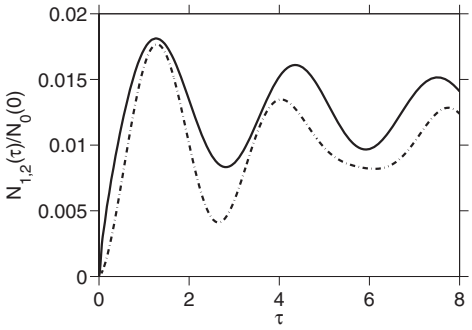

FIG. 4. Comparison of the results obtained without (solid line) and with (dashed-dotted line) the flat density-of-states approximation in 3D. In both cases we set $|\delta|=1$ and $N_0/l^3=3.1$, corresponding to $\Upsilon=3\times10^4$. For the dashed-dotted line, only the value of Υ matters, and the same curve can be obtained with different individual values of $|\delta|$ and N_0/l^3 as long as they result in the same Υ, Eq. (28).

$$\Upsilon = \frac{2N_0}{\hbar^2\kappa^2[D(\hbar|\Delta|)]^2}, \tag{27}$$

and coincides with the parameter Γ introduced in Ref. [23] (where we note that $N=2N_0$); this is the only parameter that characterizes the system at large detunings. Using Eq. (A5), Υ can be written explicitly for 1D, 2D, and 3D as follows:

$$\Upsilon = \begin{cases} 8\pi^2|\delta|N_0^2/l^2 & \text{(1D)}, \\ 32\pi^2N_0^2/l^4 & \text{(2D)}, \\ 32\pi^4N_0^2/(l^6|\delta|) & \text{(3D)}. \end{cases} \tag{28}$$

This approximation breaks down for small absolute detunings where the dissociation predominantly populates a range of atomic momenta close to zero and the density of states here can no longer be approximated as flat. As a result the system is parameterized by two variables Υ and $|\delta|$, or equivalently in terms of the original pair N_0 and $|\delta|$, without the need to introduce Υ.

In Fig. 4 we show the comparison between the results obtained with and without the use of the flat density of states approximation. In this example, the absolute dimensionless detuning is $|\delta|=1$ and we see significant discrepancy between the two curves. The discrepancy increases further for smaller detunings, while it becomes negligible for detunings $|\delta|\gtrsim 16$.

B. Indistinguishable atoms

In the case of dissociation into indistinguishable atoms our treatment corresponds to the Hamiltonian

$$\hat{H} = \sum_{\mathbf{k}} \hbar\Delta_{\mathbf{k}}\hat{a}_{1,\mathbf{k}}^{\dagger}\hat{a}_{1,\mathbf{k}} - i\frac{\hbar\kappa}{2}\sum_{\mathbf{k}}(\hat{b}_0^{\dagger}\hat{a}_{1,\mathbf{k}}\hat{a}_{1,-\mathbf{k}} - \hat{a}_{1,-\mathbf{k}}^{\dagger}\hat{a}_{1,\mathbf{k}}^{\dagger}\hat{b}_0), \tag{29}$$

where again $\kappa\equiv\chi_D/L^{D/2}$ and χ_D $(D=1,2,3)$ are given by Eqs. (7), (3), and (4).

The analysis of this system within the PMFT is essentially the same as in the distinguishable case, Eqs. (23). The only

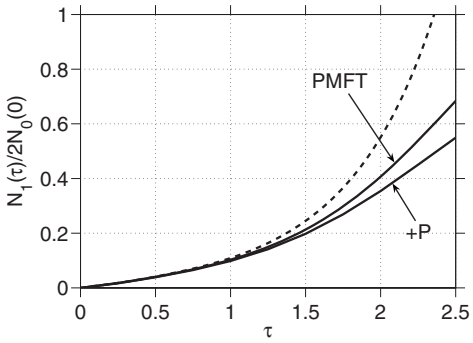

FIG. 5. Fractional atomic population $N_1(\tau)/2N_0(0)$ in 3D obtained using the present pairing mean-field theory and first-principles (exact) simulations of the same system using the positive-P representation method (+P) [24]. The dashed line corresponds to the undepleted molecular field approximation. The parameter values are $|\delta|=4$ and $N_0(0)/l^3=0.988$.

difference is in the equation for $f(\tau)$, which now reads as

$$\frac{df(\tau)}{d\tau} = -\frac{1}{2\beta_0^2}\sum_{\mathbf{k}} m_{\mathbf{k}}(\tau), \tag{30}$$

while the normal and anomalous populations are

$$n_{\mathbf{k}}(t) \equiv \langle \hat{n}_{1,\mathbf{k}}(t)\rangle = \langle \hat{a}^{\dagger}_{1,\mathbf{k}}(t)\hat{a}_{1,\mathbf{k}}(t)\rangle, \tag{31}$$

$$m_{\mathbf{k}}(t) \equiv \langle \hat{m}_{\mathbf{k}}(t)\rangle = \langle \hat{a}_{1,\mathbf{k}}(t)\hat{a}_{1,-\mathbf{k}}(t)\rangle. \tag{32}$$

In Fig. 5 we show a comparison between the present pairing mean-field theory and first-principles (exact) simulations of the same system using the positive-P representation method [24]. As we see, the pairing mean-field theory compares well with the exact results for dissociation durations corresponding to less than 50% conversion at which stage the discrepancy reaches ~20%. This is much better than the results obtained using the undepleted molecular field approximation [24], shown by the dashed line.

We note, however, that the comparison between the PMFT results and those of the positive-P method are not entirely equivalent as the positive-P method takes into account the possibility of a dynamical population of the initially unoccupied molecular modes with nonzero momenta. As has been shown in Ref. [24], this process becomes a sizeable effect as time progresses and occurs due to "rogue" association in which a small fraction of newly formed atoms convert back into molecules with nonzero momenta. The present version of the pairing mean-field scheme only treats the molecular condensate mode $\hat{b}_0$ [see Eq. (18)] without allowing for population of the noncondensate modes $\hat{b}_{\mathbf{k}}$ ($\mathbf{k} \neq 0$) present in the original Hamiltonian (17). The performance of the PMFT can be improved (at the cost of increased computational complexity) by incorporating the mean-field dynamics of all noncondensate modes $\langle \hat{b}_{\mathbf{k}}(t)\rangle \rightarrow \beta_{\mathbf{k}}(t)$, irrespective of their initial population. In this manner one can extend the present treatment from uniform to physically more realistic nonuniform systems corresponding to spatially inhomogeneous trapped condensates. This will be considered in future work.

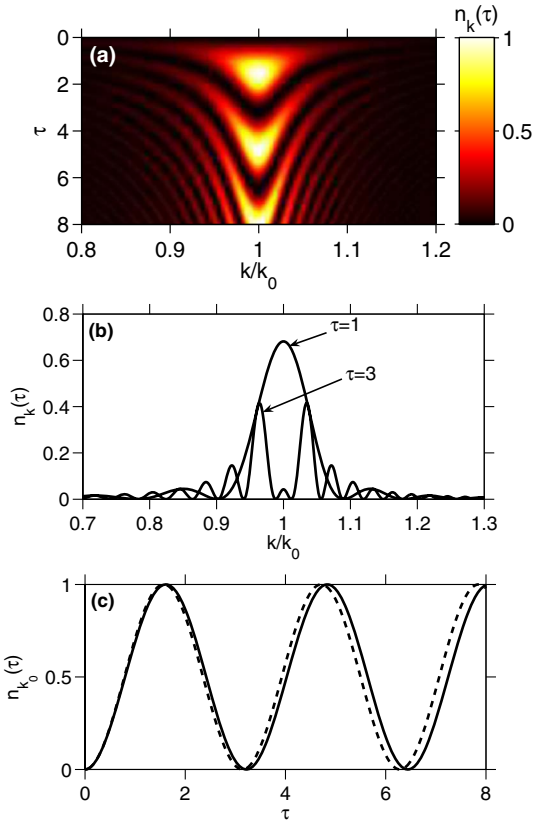

FIG. 6. (Color online) Atomic momentum distribution in each spin state for dissociation into fermionic atoms for a dimensionless absolute detuning $|\delta|=|\Delta|t_0=16$ and $N_0(0)/l^D=3.1$. Only the range of momenta whose population is nonvanishing is shown. (a) $n_{\mathbf{k}}(\tau)$ as a function of scaled time $\tau=t/t_0$ and scaled absolute momentum k/k_0 in 3D. (b) Time slices of the momentum distribution at $\tau=1$ and $\tau=3$. (c) Temporal population of the resonant momentum mode with $k=k_0$. The dashed line represents the respective analytic solution given by $\sin^2(\tau)$ in the undepleted molecular field approximation [50].

V. MOMENTUM DISTRIBUTION AND ATOM-ATOM CORRELATIONS

A. Atomic momentum distribution

In this section we analyze the momentum distribution of the dissociated atoms, $n_{\mathbf{k}}(t)$, which is the same for both spin states. In Fig. 6(a) we plot the momentum distribution versus time for the case of fermionic atom statistics. Due to the spherical symmetry in 3D, we only show the radial dependence on the absolute momentum $k=|\mathbf{k}|$, scaled with respect to the resonant momentum $k_0=\sqrt{2m_1|\Delta|}/\hbar$.

In Fig. 6(b) we show examples of snapshots of the momentum distribution at times $\tau=1$ and $\tau=3$. The respective 1D and 2D results are very similar to the 3D results and are not shown. The maximum deviation from the 3D result is in the 1D case and is less than 2% at $\tau=3$.

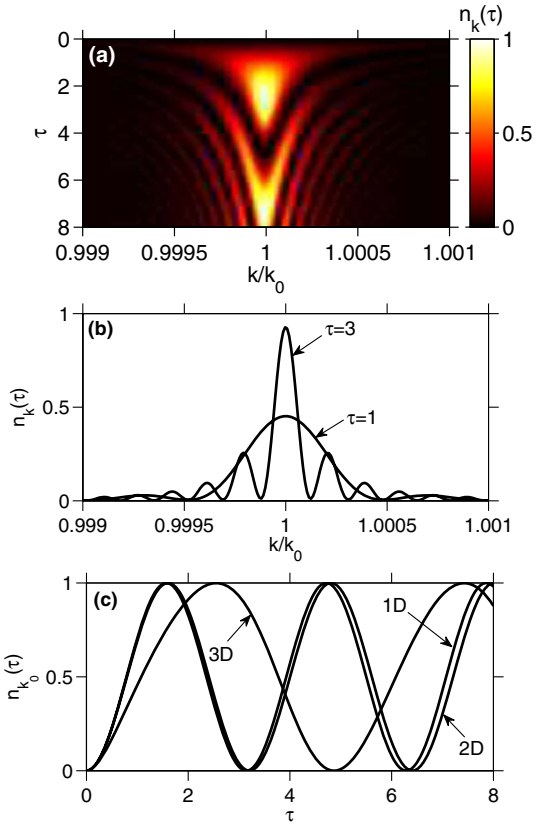

FIG. 7. (Color online) Same as in Fig. 6 except for $|\delta|=3174$. In (c) we show the temporal population of the resonant mode k_0 in 1D, 2D, and 3D. The analytic result of $\sin^2(\tau)$ corresponding to the undepleted molecular field approximation is practically identical to the 1D curve shown.

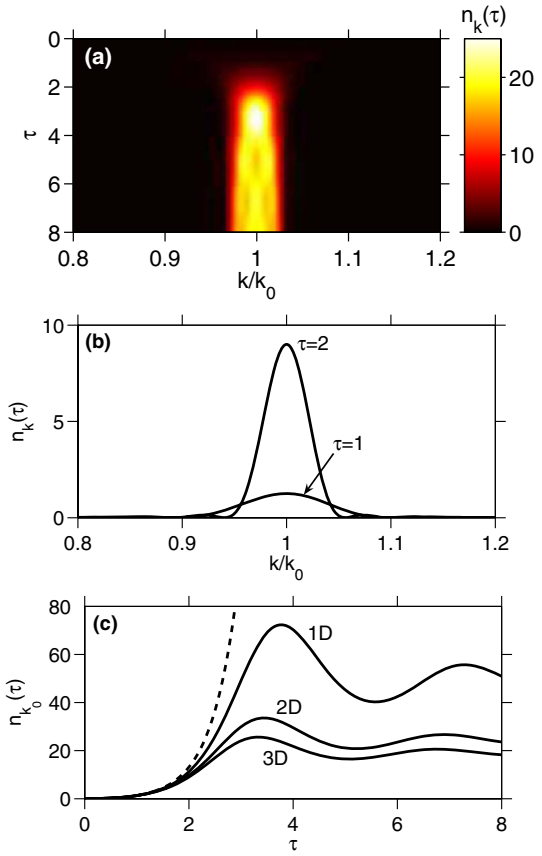

FIG. 8. (Color online) Same as in Fig. 6 ($|\delta|=16$) except for bosonic statistics of the atoms. The time slices of the momentum distribution in (b) are for $\tau=1$ and $\tau=2$. In (c), we show the temporal population of the resonant mode k_0 in 1D, 2D, and 3D (solid line), together with the respective analytic result, $\sinh^2(\tau)$ (dashed line), obtained using the undepleted molecular field approximation [50].

In Fig. 6(c) we plot the occupation of the resonant mode k_0 as a function of time. The dashed line is the analytic result obtained using the undepleted molecular field approximation given by $\sin^2(\tau)$, and is applicable in all dimensions [50]. Again the 1D and 2D results of the present pairing mean-field theory are omitted for clarity—in the 1D case the result is almost indistinguishable from the dashed line, while in 2D it is intermediate between the dashed line and the 3D solid line. The larger discrepancy of the 3D result from the approximate analytic solution is explained by the fact that molecular depletion is a more significant effect in 3D. This is better seen in Fig. 7 for the significantly larger absolute detuning $|\delta|$, where the molecular depletion is more important and hence the discrepancy between the pairing mean-field result and that of the undepleted molecular field approximation is larger.

Figures 8 and 9 are the results for the same parameters as in Figs. 6 and 7, respectively, except that they are for bosonic atom statistics. Compared to the fermionic case of Fig. 6, the dissociation dynamics in Fig. 8 are not affected by the Pauli exclusion principle and we see larger discrepancies between the 1D, 2D, and 3D results. The disagreement between the undepleted molecular field approximation and that of the present PMFT is again largest in the 3D case due to the larger density of states which results in faster depletion.

It is instructive to use the above numerical results to determine the width of the shell of the dissociation sphere and compare it with the predictions of much simpler analytic approaches. By doing this we can get a better understanding of the validity of these approximate methods. For example, the simplest estimate of the width of the dissociation sphere can be obtained from energy-time uncertainty considerations. More specifically, for short duration of dissociation t ($\Gamma t \ll 1$) during which the dissociation is in the spontaneous regime and is independent of atom statistics, the width of the dissociation sphere can be obtained through the relation $\Delta E t \sim \hbar$. Here, the energy uncertainty is evaluated in terms of the momentum uncertainty Δk around the resonant momentum $k_0 = \sqrt{2m_1|\Delta|}/\hbar$,

$$\Delta E = \frac{\hbar^2(k_0+\Delta k)^2}{2m_1} - \frac{\hbar^2 k_0^2}{2m_1} \simeq \frac{\hbar^2 k_0 \Delta k}{m_1}, \tag{33}$$

where we assumed $\Delta k/k_0 \ll 1$. According to this, the momentum uncertainty Δk which gives the width of the dissociation sphere is given by

$$\frac{\Delta k}{k_0} \simeq \frac{m}{\hbar k_0^2 t} = \frac{1}{2|\Delta|t} = \frac{1}{2|\delta|\tau}, \tag{34}$$

which is inversely proportional to the duration of dissociation t as expected and also to k_0^2 (or $|\Delta|$), implying that for

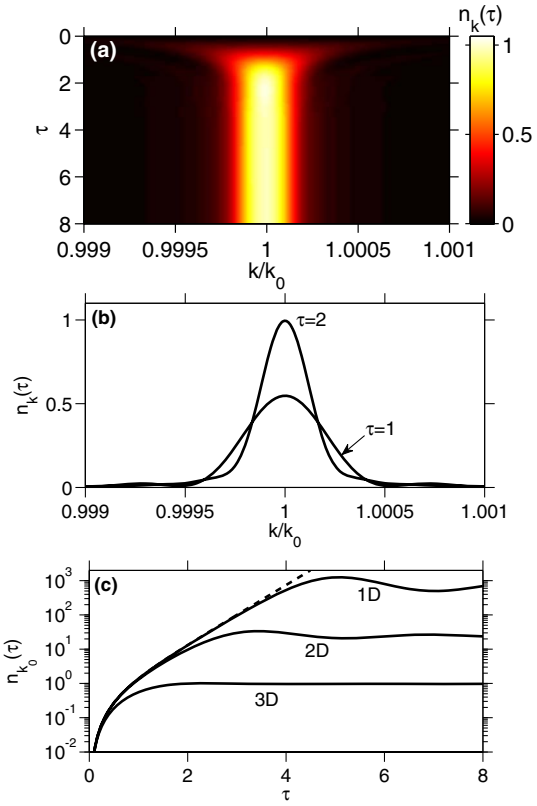

FIG. 9. (Color online) Same as in Fig. 7 ($|\delta|=3174$) except for bosonic atom statistics.

larger detuning $|\Delta|$ the width of the sphere is narrower. These conclusions are clearly seen from our numerical results for $\tau \lesssim 1$, shown in Figs. 6–9. For example, at $\tau=1$ we obtain [from Eq. (34)] $\Delta k/k_0 \simeq 0.03$ for $|\delta|=16$ and $\Delta k/k_0 \simeq 1.6 \times 10^{-4}$ for $|\delta|=3174$, in good agreement with the numerical results of Figs. 6(b), 7(b), 8(b), and 9(b).

For longer duration of dissociation, when the dynamics is strongly affected by either Bose stimulation or Pauli blocking, the width of the dissociation sphere can be estimated (see Appendix D) using a slightly more involved approach based on analytic solutions within the undepleted molecular BEC approximation [24,50]. In the fermionic case, where the momentum spectrum develops oscillatory peaks, the width in question is for the envelope function. Apart from this distinction between the fermionic and bosonic results, the width of the dissociation spherical shell is the same in the two cases and is given by

$$\frac{\Delta k}{k_0} \simeq \frac{m\chi_D\sqrt{N_0/L^D}}{2\hbar k_0^2} = \frac{1}{4|\delta|}. \tag{35}$$

This is still inversely proportional to the dimensionless detuning $|\delta|$, but no longer depends on time as the momentum distribution in this regime ($\tau \gtrsim 2$ in most of our examples) settles into a shape with an approximately constant (envelope) width and residual oscillations (see Figs. 6–9). For $|\delta|=16$ and $|\delta|=3174$, the above expression gives, respectively, $\Delta k/k_0=0.016$ and $\Delta k/k_0=0.79\times 10^{-4}$ which are again in good agreement with the numerical results.

B. Atom-atom correlations

1. Distinguishable case

In this section we study the correlation between the occupation number fluctuations for atoms in opposite spin states

$$G_{12}(\mathbf{k},\mathbf{k}',t) = \frac{\langle \Delta\hat{n}_{1,\mathbf{k}}(t)\Delta\hat{n}_{2,\mathbf{k}'}(t)\rangle}{\langle \hat{n}_{1,\mathbf{k}}(t)\rangle^{1/2}\langle \hat{n}_{2,\mathbf{k}'}(t)\rangle^{1/2}} = \frac{\langle \hat{n}_{1,\mathbf{k}}(t)\hat{n}_{2,\mathbf{k}'}(t)\rangle - \langle \hat{n}_{1,\mathbf{k}}(t)\rangle\langle \hat{n}_{2,\mathbf{k}'}(t)\rangle}{\langle \hat{n}_{1,\mathbf{k}}(t)\rangle^{1/2}\langle \hat{n}_{2,\mathbf{k}'}(t)\rangle^{1/2}}, \tag{36}$$

where $\Delta\hat{n}_{j,\mathbf{k}}(t)=\hat{n}_{j,\mathbf{k}}(t)-\langle \hat{n}_{j,\mathbf{k}}(t)\rangle$ is the fluctuation. The definition of G_{12} is different from the more conventional Glauber second-order correlation function [63]

$$g_{12}^{(2)}(\mathbf{k},\mathbf{k}',t) = \frac{\langle \hat{a}_{1,\mathbf{k}}^{\dagger}(t)\hat{a}_{2,\mathbf{k}'}^{\dagger}(t)\hat{a}_{2,\mathbf{k}'}(t)\hat{a}_{1,\mathbf{k}}(t)\rangle}{\langle \hat{n}_{1,\mathbf{k}}(t)\rangle\langle \hat{n}_{2,\mathbf{k}'}(t)\rangle}, \tag{37}$$

in that G_{12} is normalized to the square root of the product of the occupation numbers (rather than to the direct product) and the contribution from uncorrelated statistics is subtracted from it so that absence of correlation corresponds to $G_{12}=0$. The above definition of G_{12} has been used in Ref. [5] for quantifying the strength of correlation between the atoms in two hyperfine states of ^{40}K atoms created through molecular dissociation, and it is particularly convenient for fermionic atom statistics since in this case G_{12} is bounded between 0 and 1. The correlation functions G_{12} and $g_{12}^{(2)}$ are related by a simple relationship,

$$g_{12}^{(2)}(\mathbf{k},\mathbf{k}',t) = 1 + \frac{G_{12}(\mathbf{k},\mathbf{k}',t)}{\langle \hat{n}_{1,\mathbf{k}}(t)\rangle^{1/2}\langle \hat{n}_{2,\mathbf{k}'}(t)\rangle^{1/2}}. \tag{38}$$

Using Wick's theorem to factor higher-order correlation functions and express them in terms of the normal and anomalous populations, $\langle \hat{a}_{i,\mathbf{k}}^{\dagger}(t)\hat{a}_{j,\mathbf{k}'}(t)\rangle$ and $\langle \hat{a}_{i,\mathbf{k}}(t)\hat{a}_{j,\mathbf{k}'}(t)\rangle$, we find, in particular, that the correlation between the atoms with equal but opposite momenta, $\mathbf{k}'=-\mathbf{k}$, is given by

$$G_{12}(\mathbf{k},-\mathbf{k},t) = \frac{|m_{\mathbf{k}}(t)|^2}{n_{\mathbf{k}}(t)} = 1 \pm n_{\mathbf{k}}(t). \tag{39}$$

Here, the upper (lower) sign refers to bosonic (fermionic) statistics, and we have used the fact that in the present pairing mean-field theory any second-order moments other than those in Eqs. (20) and (21) are zero. In addition, we have used Eq. (25) for expressing the anomalous occupation $m_{\mathbf{k}}(t)$ via the normal occupation number $n_{\mathbf{k}}(t)$. This gives the maximum possible value of the anomalous moment $m_{\mathbf{k}}$ and hence the maximum strength of the second-order correlation function between the atoms with opposite momenta [24,50]. Therefore, the results of the present (approximate) PMFT for correlation functions give the respective upper bounds to their exact values.

For any $\mathbf{k}' \neq -\mathbf{k}$, on the other hand, we have

$$G_{12}(\mathbf{k},\mathbf{k}',t) = 0, \quad \mathbf{k}' \neq -\mathbf{k} \tag{40}$$

which corresponds to absence of any correlation.

For completeness, we also give the results for the correlation between the occupation fluctuations for the atoms in the same spin state,

$$G_{jj}(\mathbf{k},\mathbf{k}',t) = \frac{\langle \Delta\hat{n}_{j,\mathbf{k}}(t)\Delta\hat{n}_{j,\mathbf{k}'}(t)\rangle}{\langle \hat{n}_{j,\mathbf{k}}(t)\rangle^{1/2}\langle \hat{n}_{j,\mathbf{k}'}(t)\rangle^{1/2}}. \tag{41}$$

For the present pairing mean-field theory, this is given by

$$G_{11}(\mathbf{k},\mathbf{k}',t) = G_{22}(\mathbf{k},\mathbf{k}',t) = \begin{cases} \pm n_{\mathbf{k}}(t), & \mathbf{k}' = \mathbf{k}, \\ 0, & \mathbf{k}' \neq \mathbf{k}, \end{cases} \tag{42}$$

where again the upper (lower) sign refers to bosonic (fermionic) statistics. Here, the case with $\mathbf{k}' \neq \mathbf{k}$ implies uncorrelated statistics, which in terms of Glauber's second-order correlation function corresponds to $g_{11}^{(2)}(\mathbf{k},\mathbf{k}' \neq \mathbf{k},t)=1$. Similarly, $G_{11}(\mathbf{k},\mathbf{k},t)=n_{\mathbf{k}}(t)$ in the bosonic case corresponds to the level of correlations between thermally bunched atoms, $g_{11}^{(2)}(\mathbf{k},\mathbf{k},t)=2$. Finally, $G_{11}(\mathbf{k},\mathbf{k},t)=-n_{\mathbf{k}}(t)$ in the fermionic case corresponds to $g_{11}^{(2)}(\mathbf{k},\mathbf{k},t)=0$ implying perfect antibunching, which is a simple consequence of the Pauli exclusion principle.

The result of Eq. (39) for the opposite spin atoms corresponds to

$$g_{12}^{(2)}(\mathbf{k},-\mathbf{k},t) = 1 + \frac{1 \pm n_{\mathbf{k}}(t)}{n_{\mathbf{k}}(t)}. \tag{43}$$

Thus, strong correlation between the atoms with equal but opposite momenta corresponds to $g_{12}^{(2)}(\mathbf{k},-\mathbf{k},t)=1/n_{\mathbf{k}}(t)>1$ in the fermionic case, with $n_{\mathbf{k}}(t)<1$ due to Pauli blocking, and to $g_{12}^{(2)}(\mathbf{k},-\mathbf{k},t)=2+1/n_{\mathbf{k}}(t)>2$ in the bosonic case, corresponding to super-thermal bunching.

Since Wick's factorization scheme as employed here is equally valid for the pairing mean-field theory and for the treatment of Ref. [50] with the undepleted molecular field approximation, all results for second-order correlation functions obtained in Ref. [50] remain valid here. The only difference is that the analytic solutions for $n_{\mathbf{k}}(t)$ [50] are now replaced by the numerical solution of Eqs. (23). This takes into account molecular depletion and therefore the present results are expected to be more accurate.

2. Indistinguishable case

In the case of molecular dissociation into bosonic atom pairs in the same spin state, the considerations and analysis of the preceding section remain valid, except that the role of $G_{12}(\mathbf{k},-\mathbf{k},t)$ is now taken by $G_{11}(\mathbf{k},-\mathbf{k},t)$. We note, however, that for indistinguishable atoms the conveniences associated with using $G_{11}(\mathbf{k},\mathbf{k}',t)$—as inEq. (41)—for characterizing the strength of correlation between atom pairs are no longer valid. For example, in the present pairing mean-field theory we find that the correlation functions $G_{11}(\mathbf{k},-\mathbf{k},t)$ and $G_{11}(\mathbf{k},\mathbf{k},t)$ are both equal to $1+n_{\mathbf{k}}(t)$, which does not distinguish between the strength of correlation for atom pairs with opposite momenta and the strength of autocorrelation signal. For this reason, we use Glauber's second-order correlation function

$$g_{11}^{(2)}(\mathbf{k},\mathbf{k}',t) = \frac{\langle \hat{a}_{1,\mathbf{k}}^{\dagger}(t)\hat{a}_{1,\mathbf{k}'}^{\dagger}(t)\hat{a}_{1,\mathbf{k}'}(t)\hat{a}_{1,\mathbf{k}}(t)\rangle}{\langle \hat{n}_{1,\mathbf{k}}(t)\rangle\langle \hat{n}_{1,\mathbf{k}'}(t)\rangle}. \tag{44}$$

Following the same arguments as in Ref. [24], we obtain the following results:

$$g_{11}^{(2)}(\mathbf{k},\mathbf{k}',t) = \begin{cases} 1, & \mathbf{k}' \neq \mathbf{k},\ \mathbf{k}' \neq -\mathbf{k}, \\ 2, & \mathbf{k}' = \mathbf{k} \neq 0, \\ 2 + 1/n_{\mathbf{k}}(t), & \mathbf{k}' = -\mathbf{k}, \\ 3 + 1/n_{\mathbf{k}}(t), & \mathbf{k}' = \mathbf{k} = 0, \end{cases} \tag{45}$$

which again formally coincide with those obtained using the undepleted molecular field approximation [24], except that the mode occupation numbers $n_{\mathbf{k}}(t)$ are now given by the numerical solutions of the present pairing mean-field theory, Eqs. (23) and (30).

C. Correlations in column densities in 3D systems

The correlation functions derived and discussed in the preceding section are difficult to measure experimentally. Rather than density functions such as $n(\mathbf{x})$ being measured in the laboratory, column densities such as $\int dz n(\mathbf{x})$ are obtained using the technique of absorption imaging. Indeed, the correlation measurements performed in the experiments at JILA on dissociation of a molecular condensate of $^{40}K_2$ dimers into fermionic atom pairs [5] were made using absorption images after a time-of-flight expansion. We now analyze the momentum space analog of this procedure and calculate the correlation between momentum column density fluctuations.

First, we define the atom number operator corresponding to a z-integrated momentum column density, $\hat{\bar{n}}_{j,\mathbf{p}}=\Sigma_{k_z}\hat{n}_{j,\mathbf{k}}$, where $\mathbf{p}\equiv(k_x,k_y)$ is the reduced 2D momentum. The average column density $\bar{n}_{\mathbf{p}}(t)=\langle \hat{\bar{n}}_{j,\mathbf{p}}(t)\rangle$ is found via $\bar{n}_{\mathbf{p}}(t)=\Sigma_{k_z}n_{\mathbf{k}}(t)$ and is the same for the two spin states, $j=1,2$. The correlation function between the momentum column density fluctuations in the two spin states, which we denote via $\bar{G}_{12}(\mathbf{k},\mathbf{k}',t)$, is defined as in Eq. (36) except that the operators $\hat{n}_{j,\mathbf{k}}$ are replaced by $\hat{\bar{n}}_{j,\mathbf{p}}$,

$$\bar{G}_{12}(\mathbf{p},\mathbf{p}',t) = \frac{\langle \Delta\hat{\bar{n}}_{1,\mathbf{p}}(t)\Delta\hat{\bar{n}}_{2,\mathbf{p}'}(t)\rangle}{\langle \hat{\bar{n}}_{1,\mathbf{p}}(t)\rangle^{1/2}\langle \hat{\bar{n}}_{2,\mathbf{p}'}(t)\rangle^{1/2}}. \tag{46}$$

We emphasize that the summation over the k_z component must be performed before taking the ensemble average.

Using Wick's theorem as before, we obtain the following results for equal but opposite momenta, $\mathbf{p}'=-\mathbf{p}$:

$$\bar{G}_{12}(\mathbf{p},-\mathbf{p},t) = 1 \pm \frac{\sum_{k_z}[n_{\mathbf{k}}(t)]^2}{\bar{n}_{\mathbf{p}}(t)}. \tag{47}$$

Here the plus sign stands for bosons, while the minus sign is for fermions, and the distinction between the bosonic and fermionic results is highlighted through the fact that $\bar{G}_{12}(\mathbf{p},-\mathbf{p},t)>1$ for bosons and $\bar{G}_{12}(\mathbf{p},-\mathbf{p},t)<1$ for fermions. For any other pair of momenta ($\mathbf{p}' \neq -\mathbf{p}$), the correlation function

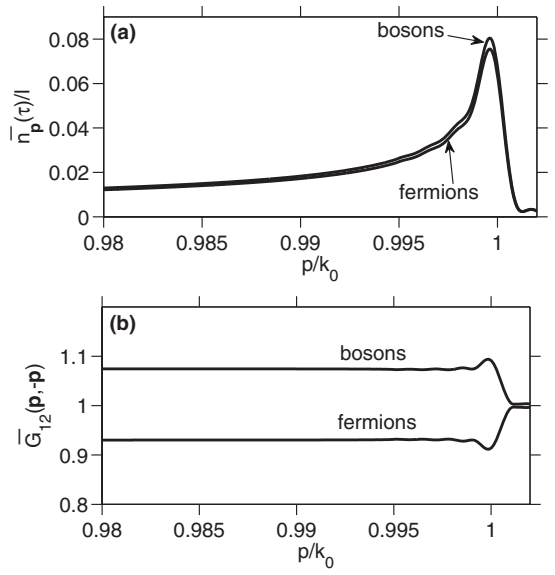

FIG. 10. (a) Momentum-space column density $\bar{n}_{\mathbf{p}}(\tau)/l$ of each spin component at $\tau=0.36$ for bosonic and fermionic cases in 3D for $|\delta|=3174$ and $N_0(0)/l^D=3.1$. The horizontal axis is the absolute value of the 2D reduced momentum $p=|\mathbf{p}|$, where $\mathbf{p}\equiv(k_x,k_y)$. (b) Correlation function between momentum column density fluctuations for the atoms with opposite spins and conjugate momenta, $\bar{G}_{12}(\mathbf{p},-\mathbf{p},\tau)$, as a function of $p=|\mathbf{p}|$, for the same parameter values as in (a).

is zero, implying the absence of any correlation.

In Fig. 10 we show examples of momentum column densities $\bar{n}_{\mathbf{p}}(t)$ and correlations between column density fluctuations $\bar{G}_{12}(\mathbf{p},-\mathbf{p},t)$ for bosonic and fermionic atoms for $|\delta|=3174$ at $\tau=0.36$. The dissociation at this stage is still in the spontaneous regime, so the difference between the column densities for bosonic and fermionic cases is hardly noticeable in Fig. 10(a). On the other hand, the difference due to quantum statistics becomes much more pronounced if one examines the pair correlation function $\bar{G}_{12}(\mathbf{p},-\mathbf{p},t)$, as shown in Fig. 10(b), with $\bar{G}_{12}(\mathbf{p},-\mathbf{p},t)>1$ for bosons and $\bar{G}_{12}(\mathbf{p},-\mathbf{p},t)<1$ for fermions.

The example of Fig. 10 in the fermionic case, with $\bar{G}_{12}(\mathbf{p},-\mathbf{p},t)\simeq 0.9$, corresponds to the experimental parameters of Ref. [5]. We note that the experimentally measured spatial counterpart of the same correlation function after time-of-flight expansion varied between 0.1 and 0.3 depending on the bin size used in the analysis of the imaged data. The dependence of the strength of the correlation signal on bin size was analyzed theoretically in Ref. [31]. However, ignoring variations due to binning, the experimental result was significantly less than our theoretically calculated value in momentum space. This highlights an important limitation of the present uniform theory, which is that it only gives the upper bound of correlation functions [50] and is not adequate for correct quantitative description of realistic nonuniform systems. This conclusion, however, does not necessarily apply to other quantities of interest, such as the momentum distribution or the total atom number. In these cases, the quantitative predictions of the uniform theory can adequately describe nonuniform systems if the uniform system is properly size matched to the nonuniform one as done in Sec. IV A 1 (see also Ref. [24]).

The reason that the PMFT gives unsatisfactory results for pair correlations is the mode mixing which couples the atomic momenta not only in a pairwise fashion, $(\mathbf{k},-\mathbf{k})$, but also couples within the neighborhood of the partners. As a result the correlations are broadened, while their strength can be dramatically reduced, especially in systems with strong inhomogeneity. The problem of mode mixing was analyzed in detail in the bosonic case in Ref. [24] using the comparison between uniform solutions and exact quantum simulations of nonuniform systems using the stochastic positive P-representation method. Performing similar first-principle quantum dynamical calculations for nonuniform, multimode fermionic systems is a challenging problem yet to be solved.

VI. CONCLUSIONS

We have developed a simple pairing mean-field theory for the quantum dynamics of the dissociation of a Bose-Einstein condensate of diatomic molecules into its constituent particles, covering the cases of indistinguishable bosons and distinguishable fermions or bosons. The pairing fields for the atoms are introduced at the level of normal and anomalous moments for the atomic creation and annihilation operators; such an approach is necessary as the dissociation is initially a spontaneous process and cannot be described by ordinary mean-field theory. We have solved the resulting equations of motion for all cases, and identified the role of dimensionality and quantum statistics on the conversion rate, and compared them to the simpler analytic solutions available within the undepleted molecular field approximation.

We find that molecular depletion is a more important effect in higher dimensions and in the case of dissociation into bosonic atoms. Accordingly, we argue that the undepleted molecular approximation is more reliable for describing dissociation into fermionic atoms and systems of reduced dimensionality. This conclusion can be useful in extensions of the theory of dissociation to spatially inhomogeneous systems. In this case, the simplest treatment would be to employ the undepleted molecular field approximation, while still being able to address the problem of mode mixing, which is the most important issue when seeking quantitative description of atom-atom correlations.

We have also compared the results in the bosonic, indistinguishable case to the exact dynamics found by positive-P simulation and identified the range of validity of the pairing mean-field theory. In addition, we have compared our formalism to that of Jack and Pu [23], and identified the key differences. Finally, we have derived and calculated results for the nontrivial correlations that are present in the dissociated atoms, and compared our results to those of the experiment performed at JILA [5].

The main limitation of this work (see also Sec. II C) is the assumption of a uniform molecular condensate. This limits the time for which the dynamics are valid and also does not allow for the association of atoms into previously unoccupied molecular modes. The PMFT can be used to describe

realistic nonuniform condensates provided the results are applied to a size-matched system. The total atom number and atomic density distribution obtained in this way can be quantitatively reasonable, however, the same is not true if the calculated quantities involve density-density correlation functions. In this case the PMFT provides upper bounds for the correlation functions. We are currently extending the PMFT to include the effects of spatial inhomogeneity to provide a quantitatively better model.

ACKNOWLEDGMENTS

The authors acknowledge support of this work by the Australian Research Council and the Queensland State Government.

APPENDIX A: DECAY RATE IN THE DISTINGUISHABLE CASE

The transition matrix element V_{ma} in Eq. (10) is

$$V_{ma} = \langle f|\hat{H}_{\rm int}|i\rangle, \tag{A1}$$

where $\hat{H}_{\rm int}$ is the atom-molecule coupling term in the Hamiltonian (1), while the initial $|i\rangle$ and final $|f\rangle$ states describe a free molecule or a pair of free atoms, respectively,

$$|i\rangle = \frac{1}{L^{D/2}}\int d^D\mathbf{x}\hat{\Psi}_0^\dagger(\mathbf{x})e^{i\mathbf{K}\cdot\mathbf{x}}|0\rangle, \tag{A2}$$

$$|f\rangle = \frac{1}{L^D}\int\int d^D\mathbf{x}d^D\mathbf{y}\hat{\Psi}_1^\dagger(\mathbf{x})\hat{\Psi}_2^\dagger(\mathbf{y})e^{i\mathbf{K}\cdot(\mathbf{x}+\mathbf{y})/2}|0\rangle. \tag{A3}$$

Here $\mathbf{K}$ is the total center-of-mass momentum, L is the quantization length in each dimension, and the states are normalized to one. Calculating the matrix element in Eq. (A1) gives

$$|V_{ma}|^2 = \frac{\hbar^2\chi_D^2}{L^D}. \tag{A4}$$

Next, the density of two-atom states $D^{(2)}(\epsilon)$ at the total dissociation energy $\epsilon=2\hbar|\Delta|$ is the same as the standard density of single-atom states $D(E)$ at energy $E=\epsilon/2$ evaluated at one-half the quantization volume $V=L^3$ for a single molecule (or area $A=L^2$ in 2D, or length L in 1D); equivalently it is the same as one-half the density of single-atom states evaluated for the same quantization volume, and is given by [51]

$$D^{(2)}(\epsilon) = \frac{1}{2}D(E) = \begin{cases} \alpha L/(2\sqrt{E}) & \text{(1D)}, \\ \pi(\alpha L)^2/2 & \text{(2D)}, \\ \pi(\alpha L)^3\sqrt{E} & \text{(3D)}, \end{cases} \tag{A5}$$

where $\alpha=(2m_1/\hbar^2)^{1/2}/2\pi$ is a constant. Combining Eqs. (10), (A4), and (A5), and expressing the final result in terms of the absolute detuning $|\Delta|$, we obtain Eq. (11) for the decay rate Γ.

APPENDIX B: DECAY RATE IN THE INDISTINGUISHABLE CASE

The initial $|i\rangle$ and final $|f\rangle$ states describing, a free molecule and a pair of free indistinguishable atoms, respectively, are

$$|i\rangle = \frac{1}{L^{D/2}}\int d^D\mathbf{x}\hat{\Psi}_0^\dagger(\mathbf{x})e^{i\mathbf{K}\cdot\mathbf{x}}|0\rangle, \tag{B1}$$

$$|f\rangle = \frac{1}{\sqrt{2}L^D}\int\int d^D\mathbf{x}d^D\mathbf{y}\hat{\Psi}_1^\dagger(\mathbf{x})\hat{\Psi}_1^\dagger(\mathbf{y})e^{i\mathbf{K}\cdot(\mathbf{x}+\mathbf{y})/2}|0\rangle, \tag{B2}$$

and are again normalized to one. Applying these to the transition matrix element $V_{ma}=\langle f|\hat{H}_{\rm int}|i\rangle$, where $\hat{H}_{\rm int}$ is the interaction term in the Hamiltonian (6), we obtain

$$|V_{ma}|^2 = \frac{\hbar^2\chi_D^2}{2L^D}. \tag{B3}$$

Accordingly, the molecular decay rate, $\Gamma'=2\pi|V_{ma}|^2D^{(2)}\times(\epsilon)/\hbar$, where $D^{(2)}(\epsilon)$ is given by Eq. (A5), takes the form of Eq. (13).

APPENDIX C: PARAMETRIZATION AT LARGE DISSOCIATION ENERGY

Following the arguments of Ref. [23] we first take the continuum limit of Eqs. (23) and convert the sums over $\mathbf{k}$ into integrals. Changing from the momentum variable to the energy $E_k=\hbar^2k^2/2m_1$ and then to $\hbar\Delta_k=E_k+\hbar\Delta$, where we recall that $\Delta<0$, we can rewrite the equation for $f(\tau)$ as

$$\frac{df(\tau)}{d\tau} = -\frac{\hbar}{\beta_0^2}\int_{-|\Delta|}^{\infty} d\Delta_k D(\hbar\Delta_k-\hbar\Delta)m_k(\tau), \tag{C1}$$

where $D(E)$ is the density of states equation (A5).

At large $|\Delta|$ the resonance condition $\Delta_k=0$ (or $E_k=\hbar|\Delta|$) leads to the population of only those atomic states that have absolute momenta $k=|\mathbf{k}|$ in a narrow range around $k_0=\sqrt{2m_1|\Delta|/\hbar}$. The density of states in this range of momenta is essentially constant and therefore $D(E_k)$ can be approximated by $D(\hbar|\Delta|)$ and be taken out of the integral in Eq. (C1). At the same time, the lower limit of the integral $(-|\Delta|)$ can be replaced by $-\infty$, which leads to the following result in terms of dimensionless parameters:

$$\frac{df(\tau)}{d\tau} \simeq -\frac{\hbar D(\hbar|\Delta|)}{\beta_0^2 t_0}\int_{-\infty}^{\infty} d\delta_k m(\delta_k,\tau), \tag{C2}$$

where $\delta_k=t_0\Delta_k/\hbar$ and $m(\delta_k,\tau)$ is a continuous function corresponding to $m_k(\tau)$ after making the variable changes.

The coefficient in front of the integral in Eq. (C2) motivates the introduction of a dimensionless parameter Υ defined via $\hbar D(\hbar|\Delta|)/(\beta_0^2t_0)\equiv\sqrt{2/\Upsilon}$ and therefore

$$\Upsilon = \frac{2\beta_0^4t_0^2}{\hbar^2[D(\hbar|\Delta|)]^2} = \frac{2N_0}{\hbar^2\kappa^2[D(\hbar|\Delta|)]^2}. \tag{C3}$$

The final explicit result for Υ in 1D, 2D, and 3D is given in Eq. (28).

APPENDIX D: WIDTH OF THE DISSOCIATION SPHERE

To estimate the width of the shell of the dissociation sphere beyond the spontaneous regime we use the analytic

solutions for a uniform system in the undepleted molecular BEC approximation [24,50]. The solution for the momentum distribution $n_{\mathbf{k}}(t)$ in the bosonic case reads as

$$n_{\mathbf{k}}(t) = \frac{g^2}{g^2 - \Delta_k^2} \sinh^2(\sqrt{g^2 - \Delta_k^2}\, t), \tag{D1}$$

where

$$g = \chi_D \sqrt{N_0/L^D}, \tag{D2}$$

$$\Delta_k \equiv \frac{\hbar k^2}{2m} - \frac{\hbar k_0^2}{2m}. \tag{D3}$$

From Eq. (D1) we see that modes with $g^2 - \Delta_k^2 > 0$ experience Bose enhancement and grow exponentially with time, and the modes with $g^2 - \Delta_k^2 < 0$ oscillate at the spontaneous noise level. The absolute momenta of the exponentially growing modes lie near the resonant momentum k_0, and therefore we can use the condition $g^2 - \Delta_k^2 = 0$ to define the width of the dissociation sphere. First we write $k = k_0 + \delta k$ and assume for simplicity that k_0 is large enough so that $\delta k \ll k_0$. Then the above condition can be approximated by

$$1 - \left(\frac{\hbar k_0 \delta k}{mg}\right)^2 \simeq 0. \tag{D4}$$

This can be solved for δk and used to define the width $\Delta k = \delta k/2$ of the dissociation sphere as

$$\frac{\Delta k}{k_0} \simeq \frac{mg}{2\hbar k_0^2} = \frac{m\chi_D \sqrt{N_0/L^D}}{2\hbar k_0^2}. \tag{D5}$$

The reason for defining it as one-half the full width δk is to make Δk closer in definition to the rms width around k_0.

For the case of fermionic statistics a similar analytic solution exists [50],

$$n_{\mathbf{k}}(t) = \frac{g^2}{g^2 + \Delta_k^2} \sin^2(\sqrt{g^2 + \Delta_k^2}\, t), \tag{D6}$$

where g and Δ_k are the same as in Eqs. (D2) and (D3). In this case the solutions for all k are oscillatory, with populations of individual modes not exceeding one due to the Pauli exclusion principle. The width of the dissociation sphere can now be defined as the width of the envelope function given by the Lorentzian $g^2/(g^2 + \Delta_k^2)$. Rewriting the width of this Lorentzian in terms of the momentum width $\Delta k = \delta k/2$, we obtain the same expression as in Eq. (D5).

[1] M. Yasuda and F. Shimizu, Phys. Rev. Lett. **77**, 3090 (1996).
[2] E. A. Burt, R. W. Ghrist, C. J. Myatt, M. J. Holland, E. A. Cornell, and C. E. Wieman, Phys. Rev. Lett. **79**, 337 (1997).
[3] B. Laburthe Tolra, K. M. O'Hara, J. H. Huckans, W. D. Phillips, S. L. Rolston, and J. V. Porto, Phys. Rev. Lett. **92**, 190401 (2004).
[4] T. Kinoshita, T. Wenger, and D. S. Weiss, Phys. Rev. Lett. **95**, 190406 (2005).
[5] M. Greiner, C. A. Regal, J. T. Stewart, and D. S. Jin, Phys. Rev. Lett. **94**, 110401 (2005).
[6] S. Fölling *et al.*, Nature (London) **434**, 481 (2005).
[7] T. Rom *et al.*, Nature (London) **444**, 733 (2006).
[8] J. Esteve, J. B. Trebbia, T. Schumm, A. Aspect, C. I. Westbrook, and I. Boushoule, Phys. Rev. Lett. **96**, 130403 (2006).
[9] C.-S. Chuu, F. Schreck, T. P. Meyrath, J. L. Hanssen, G. N. Price, and M. G. Raizen, Phys. Rev. Lett. **95**, 260403 (2005).
[10] A. Öttl, S. Ritter, M. Kohl, and T. Esslinger, Phys. Rev. Lett. **95**, 090404 (2005).
[11] M. Schellekens *et al.*, Science **310**, 648 (2005).
[12] T. Jeltes *et al.*, Nature (London) **445**, 402 (2007).
[13] A. Perrin, H. Chang, V. Krachmalnicoff, M. Schellekens, D. Boiron, A. Apsoect, and C. Westbrook, Phys. Rev. Lett. **99**, 150405 (2007).
[14] T. Campey, C. J. Vale, M. J. Davis, N. R. Heckenberg, H. Rubinsztein-Dunlop, S. Kraft, C. Zimmermann, and J. Fortágh, Phys. Rev. A **74**, 043612 (2006); S. Kraft, A. Günther, J. Fortágh, and C. Zimmermann, *ibid.* **75**, 063605 (2007).
[15] A. G. Sykes, D. M. Gangardt, M. J. Davis, K. Viering, M. G. Raizen, and K. V. Kheruntsyan, e-print arXiv:0710.5812.
[16] R. Bach, M. Trippenbach, and K. Rzażewski, Phys. Rev. A **65**, 063605 (2002); P. Ziń, J. Chwedenczuk, A. Veitia, K. Rzazewski, and M. Trippenbach, Phys. Rev. Lett. **94**, 200401 (2005).
[17] A. Perrin, C. M. Savage, V. Krachmalnicoff, D. Boiron, C. I. Westbrook, and K. V. Kheruntsyan, e-print arXiv:0712.2145.
[18] U. V. Poulsen and K. Mølmer, Phys. Rev. A **63**, 023604 (2001).
[19] K. V. Kheruntsyan and P. D. Drummond, Phys. Rev. A **66**, 031602(R) (2002); K. V. Kheruntsyan, *ibid.* **71**, 053609 (2005).
[20] A. Vardi and M. G. Moore, Phys. Rev. Lett. **89**, 090403 (2002).
[21] A. A. Norrie, R. J. Ballagh, and C. W. Gardiner, Phys. Rev. Lett. **94**, 040401 (2005); Phys. Rev. A **73**, 043617 (2006).
[22] A. M. Rey, I. I. Satija, and C. W. Clark, J. Phys. B **39**, S177 (2006); New J. Phys. **8**, 155 (2006).
[23] M. W. Jack and H. Pu, Phys. Rev. A **72**, 063625 (2005).
[24] C. M. Savage, P. E. Schwenn, and K. V. Kheruntsyan, Phys. Rev. A **74**, 033620 (2006).
[25] P. Deuar and P. D. Drummond, Phys. Rev. Lett. **98**, 120402 (2007).
[26] K. J. Challis, R. J. Ballagh, and C. W. Gardiner, Phys. Rev. Lett. **98**, 093002 (2007).
[27] C. Orzel *et al.*, Science **291**, 2386 (2001).
[28] D. C. Roberts, T. Gasenzer, and K. Burnett, J. Phys. B **35**, L113 (2002).
[29] V. A. Yurovsky and A. Ben-Reuven, Phys. Rev. A **67**, 043611 (2003).
[30] M. T. Johnsson and S. A. Haine, Phys. Rev. Lett. **99**, 010401 (2007).
[31] C. M. Savage and K. V. Kheruntsyan, Phys. Rev. Lett. **99**, 220404 (2007).

[32] H. Pu and P. Meystre, Phys. Rev. Lett. **85**, 3987 (2000).
[33] L.-M. Duan, A. Sorensen, J. I. Cirac, and P. Zoller, Phys. Rev. Lett. **85**, 3991 (2000).
[34] A. Sørensen *et al.*, Nature (London) **409**, 63 (2001).
[35] V. A. Yurovsky, Phys. Rev. A **65**, 033605 (2002).
[36] K. V. Kheruntsyan, M. K. Olsen, and P. D. Drummond, Phys. Rev. Lett. **95**, 150405 (2005).
[37] S. A. Haine and J. J. Hope, Phys. Rev. A **72**, 033601 (2005).
[38] M. K. Olsen and M. J. Davis, Phys. Rev. A **73**, 063618 (2006).
[39] B. Zhao, Z. B. Chen, J. W. Pan, J. Schmiedmayer, A. Recati, G. E. Astrakharchik, and T. Calarco, Phys. Rev. A **75**, 042312 (2007).
[40] S. T. Thompson, E. Hodby, and C. E. Wieman, Phys. Rev. Lett. **94**, 020401 (2005); T. Köhler, E. Tiesinga, and P. S. Julienne, *ibid.* **94**, 020402 (2005).
[41] S. Dürr, T. Volz, N. Syassen, G. Rempe, E. van Kempen, S. Kokkelmans, B. Verhaar, and H. Friedrich, Phys. Rev. A **72**, 052707 (2005).
[42] E. Braaten and D. Zhang, Phys. Rev. A **73**, 042707 (2006).
[43] T. M. Hanna, K. Góral, E. Witkowska, and T. Köhler, Phys. Rev. A **74**, 023618 (2006).
[44] I. Tikhonenkov and A. Vardi, Phys. Rev. Lett. **98**, 080403 (2007).
[45] S. Brouard and J. Plata, Phys. Rev. A **72**, 023620 (2005).
[46] T. Miyakawa and P. Meystre, Phys. Rev. A **74**, 043615 (2006).
[47] M. Holland, J. Park, and R. Walser, Phys. Rev. Lett. **86**, 1915 (2001); S. J. J. M. F. Kokkelmans and M. J. Holland, *ibid.* **89**, 180401 (2002); J. Javanainen *et al.*, *ibid.* **92**, 200402 (2002).
[48] A. Gilchrist, C. W. Gardiner, and P. D. Drummond, Phys. Rev. A **55**, 3014 (1997); P. Deuar and P. D. Drummond, J. Phys. A **39**, 1163 (2006).
[49] J. F. Corney and P. D. Drummond, Phys. Rev. Lett. **93**, 260401 (2004); Phys. Rev. B **73**, 125112 (2006); P. Corboz *et al.*, e-print arXiv:0707.4394.
[50] K. V. Kheruntsyan, Phys. Rev. Lett. **96**, 110401 (2006).
[51] T. Mukaiyama, J. R. Abo-Shaeer, K. Xu, J. K. Chin, and W. Ketterle, Phys. Rev. Lett. **92**, 180402 (2004).
[52] S. Dürr, T. Volz, and G. Rempe, Phys. Rev. A **70**, 031601(R) (2004).
[53] P. D. Drummond, K. V. Kheruntsyan, and H. He, J. Opt. B: Quantum Semiclassical Opt. **1**, 387 (1999); K. V. Kheruntsyan and P. D. Drummond, Phys. Rev. A **61**, 063816 (2000).
[54] P. D. Drummond, K. V. Kheruntsyan, and H. He, Phys. Rev. Lett. **81**, 3055 (1998); K. V. Kheruntsyan and P. D. Drummond, Phys. Rev. A **58**, R2676 (1998); **58**, 2488 (1998).
[55] D. J. Heinzen, R. H. Wynar, P. D. Drummond, and K. V. Kheruntsyan, Phys. Rev. Lett. **84**, 5029 (2000).
[56] E. Timmermans, P. Tommasini, R. Cote, M. Hussein, and A. Kerman, Phys. Rev. Lett. **83**, 2691 (1999); Phys. Rep. **315**, 199 (1999).
[57] P. D. Drummond and K. V. Kheruntsyan, Phys. Rev. A **70**, 033609 (2004).
[58] J. Javanainen and M. Mackie, Phys. Rev. A **59**, R3186 (1999).
[59] R. A. Duine and H. T. C. Stoof, Phys. Rep. **396**, 115 (2004).
[60] T. Köhler, K. Góral, and P. S. Julienne, Rev. Mod. Phys. **78**, 1311 (2006).
[61] F. H. Mies, E. Tiesinga, and P. S. Julienne, Phys. Rev. A **61**, 022721 (2000).
[62] Notationally, the equivalence is established by noting that the detuning ν of Ref. [23] corresponds to $-\Delta$ used here. In addition, we have found the following typographical errors in Ref. [23]: (i) in Eq. (1), ν should be replaced by 2ν, and (ii) in Figs. 2 and 3, the scale on the horizontal axis should read as time $(1/g\sqrt{N})$, which corresponds to $1/(\kappa\sqrt{2|\beta_0|^2})$ in our notation.
[63] R. J. Glauber, Phys. Rev. **130**, 2529 (1963); M. Naraschewski and R. J. Glauber, Phys. Rev. A **59**, 4595 (1999).